ILMATIETEEN LAITOS
METEOROLOGISKA INSTITUTET
FINNISH METEOROLOGICAL INSTITUTE

RAPORTTEJA
RAPPORTER
REPORTS
2021:5

INFLUENCE OF FOREST FLOOR VEGETATION ON THE TOTAL FOREST REFLECTANCE AND ITS IMPLICATIONS FOR LAI ESTIMATION USING VEGETATION INDICES

TERHIKKI MANNINEN
PAULINE STENBERG

Influence of forest floor vegetation on the total forest reflectance and its implications for LAI estimation using vegetation indices

Terhikki Manninen[1] and Pauline Stenberg[2]
[1]*Finnish Meteorological Institute, PO Box 503, FI-00101 Helsinki, Finland*
[2]*Department of Forest Sciences, PO Box 27, FI-00014 University of Helsinki, Finland*

ILMATIETEEN LAITOS
METEOROLOGISKA INSTITUTET
FINNISH METEOROLOGICAL INSTITUTE

Published by **Finnish Meteorological Institute**
(Erik Palménin aukio 1), P.O. Box 503
FIN-00101 Helsinki, Finland

Series title, number and report code of publication
Raportteja - Rapporter - Reports 2021:5
Date
August 2021

Author(s)
Terhikki Manninen
Pauline Stenberg (University of Helsinki)

ORCID iD (0000-0001-8945-9122)

Title

Influence of forest floor vegetation on the total forest reflectance and its implications for LAI estimation using vegetation indices

Abstract

Recently a simple analytic canopy bidirectional reflectance factor (BRF) model based on the spectral invariants theory was presented. The model takes into account that the recollision probability in the forest canopy is different for the first scattering than the later ones. Here this model is extended to include the forest floor contribution to the total forest BRF. The effect of the understory vegetation on the total forest BRF as well as on the simple ratio (SR) and the normalized difference (NDVI) vegetation indices is demonstrated for typical cases of boreal forest. The relative contribution of the forest floor to the total BRF was up to 69 % in the red wavelength range and up to 54 % in the NIR wavelength range. Values of SR and NDVI for the forest and the canopy differed within 10 % and 30 % in red and within 1 % and 10 % in the NIR wavelength range. The relative variation of the BRF with the azimuth and view zenith angles was not very sensitive to the forest floor vegetation. Hence, linear correlation of the modelled total BRF and the Ross-thick kernel was strong for dense forests (R2 > 0.9). The agreement between modelled BRF and satellite-based reflectance values was good when measured LAI, clumping index and leaf single scattering albedo values for a boreal forest were used as input to the model.

Publishing unit
Meteorological research, Finnish Meteorological Institute

Classification (UDC)
550.34.01, 551.521.14, 630*111

Keywords
Forest, reflectance, leaf area index, model

ISSN and series title
0782-6079 Raportteja – Rapporter – Reports

ISBN
978-952-336-137-9

DOI
10.35614/isbn.9789523361379

Language
English

Pages
42

ILMATIETEEN LAITOS
METEOROLOGISKA INSTITUTET
FINNISH METEOROLOGICAL INSTITUTE

Julkaisija **Ilmatieteen laitos**
(Erik Palménin aukio 1)
PL 503, 00101 Helsinki

Julkaisun sarja, numero ja raporttikoodi
Raportteja - Rapporter - Reports 2021:5
Päiväys
Elokuu 2021

Tekijä(t)
Terhikki Manninen
Pauline Stenberg (Helsingin yliopisto)

ORCID iD (0000-0001-8945-9122, 0000-0001-5488-0857)

Nimeke
Metsän pohjakasvillisuuden vaikutus metsän heijastuskertoimeen ja sen vaikutus lehtialaindeksin arviointiin kasvillisuusindeksien avulla

Tiivistelmä
Hiljattain on esitetty yksinkertainen analyyttinen puuston kaksisuuntaisen heijastuskertoimen (BRF) malli, joka perustuu spketristä riippumattomien parametrien teoriaan. Mallissa otetaan huomioon, että fotonin uudelleen siroamisen todennäköisyys metsässä poikkeaa ensimmäisellä kerralla sen myöhemmistä arvoista. Tässä tutkimuksessa mallia on edelleen kehitetty siten, että siinä huomioidaan metsän pohjan osuus metsän BRF:stä. Aluskasvillisuuden vaikutusta BRF:ään ja kasvillisuusindekseihin SR (yksinkertainen suhde) ja NDVI (normalisoitu kasvillisuuden erotusindeksi) havainnollistetaan esimerkeillä tyypillisestä boreaalisesta metsästä. Metsän pohjan suhteellinen osuus BRF:stä ulottui 69 prosenttiin punaisen alueen aallonpituuksilla ja 54 prosenttiin lähi-infrapunan aallonpituusalueella. Metsälle laskettujen SR:n ja NDVI:n arvot poikkesivat pelkälle puustolle lasketuista vastaavista arvoista 10 % ja 30 % punaisella aallonpituusalueella ja 1 % ja 10 % lähi-infrapunan aallonpituusalueella. BRF:n suhteellinen muutos katselukulmien vaihdellessa ei ollut kovin herkkä metsän pohjakasvillisuudelle. Siten mallinnettu metsän BRF oli lineaarisesti verrannollinen Ross:n tiheän metsän kerneliin (selitysaste > 0.9). Mallinnettu BRF ja satellidatasta peräisin olevat reflektanssiarvot vastasivat hyvin toisiaan, kun mallin syöttötietoina käytettiin boreaalisen metsän mitattuja lehtialaindeksin, ryhmittyneisyysindeksin ja lehden albedon arvoja.

Julkaisijayksikkö
Meteorologinen tutkimus, Ilmatieteen laitos

Luokitus (UDK)
550.34.01, 551.521.14, 630*111

Asiasanat
Metsä, heijastuskerroin, lehtialaindeksi, malli

ISSN ja avainnimeke
0782-6079 Raportteja – Rapporter – Reports

ISBN
978-952-336-137-9

DOI
10.35614/isbn.9789523361379

Kieli
Englanti

Sivumäärä
42

ILMATIETEEN LAITOS
METEOROLOGISKA INSTITUTET
FINNISH METEOROLOGICAL INSTITUTE

Utgivare
Meteorologiska institutet
(Erik Palméns plats 1)
PB 503, 00101 Helsingfors

Publikationens serie och nummer
Raportteja - Rapporter - Reports 2021:5
Datum
Augusti 2021

Författare
Terhikki Manninen
Pauline Stenberg (Helsingfors Universitet)

ORCID iD (0000-0001-8945-9122, 0000-0001-5488-0857)

Rubrik
Inverkan av skogsbottnets undervegetation på skogens totala reflektans och dess konsekvenser för uppskattningen av bladyteindex (LAI) med hjälp av vegetationsindex

Sammandrag
En enkel analytisk modell att beräkna den dubbelriktade reflektionsfaktorn (BRF) från ett skogsbestånd baserad på teorin om spektrala invarianter presenterades nyligen. Modellen tar i betraktande att ”återkollisionssannolikheten”, eller sannolikheten för att en foton som spritts från ett fytoelement skall kollidera inom kronverket på nytt, är olik efter den första spridningen än de senare. Här utvidgas denna modell till att omfatta skogsbottnets bidrag till skogens totala BRF. Effekten av undervegetationen på skogens BRF såväl som på vegetationsindexen SR (enkelt förhållande) och NDVI (normaliserad differens) demonstreras för typiska fall av boreal skog. Skogsbottnets relativa bidrag till skogens totala BRF var upp till 69 % i det röda och upp till 54 % i det närinfraröda (NIR) våglängdsområdet. Skillnaden i värdena av SR och NDVI för hela skogen respektive kronverket varierade mellan 10 % och 30 % i det röda och mellan 1 % och 10 % i NIR våglängdesområdet. Den relativa variationen i BRF med betraktelsevinkel påverkades inte speciellt av undervegetationen. Den linjära korrelation mellan modellerad BRF och BRF genererad med ’Ross-thick kernel’ formeln var därför stark för täta skogar (R2> 0,9). Modellerade BRF överenstämde väl med satellitbaserade reflektansvärden då uppmätta värden på LAI, sammanklumpningsindex och bladens (barrens) spektrala albedo för en boreal skog användes som input till modellen.

Publikationsenhet
Meteorologi, Meteorologiska Institutet

Klassificering (UDK)
550.34.01, 551.521.14, 630*111

Nyckelord
Skog, reflektans, bladyteindex, modell

ISSN ja och serietitel
0782-6079 Raportteja – Rapporter – Reports

ISBN
978-952-336-137-9

DOI
10.35614/isbn.9789523361379

Språk
Engelska

Sidantal
42

1. Introduction

Leaf area index (*LAI*) is an essential climate variable (ECV) critical for land surface and climate modelling studies [1]. Atmospheric processes are intrinsically linked to the biosphere through the surface energy balance [2]. The important atmosphere-biosphere feedbacks to climate change predictions need to be better understood and simulated. Including the effects of changes in *LAI* on the mean annual streamflow and runoff has been shown to be important in future projections of streamflow when applying a hydrological model [3]. Also improvements for monitoring droughts have been reported from assimilating *LAI* into a land surface model [4]. Canopy *LAI* is an important parameter for carbon uptake studies and may have either positive or negative radiative forcing depending on other forest parameters and the composition of the forest floor [5]. *LAI* is also very important for photosynthesis, and a biochemical CO_2 exchange model has been shown to be sensitive to changes in the *LAI* of boreal forest on a daily scale [6, 7]. It has been suggested already more than a decade ago that better information regarding the spatial heterogeneity of key parameters, such as *LAI*, obtained from new remote sensing techniques could markedly improve boreal ecosystem model predictions [8]. In addition, replacing the previously used biome type based land surface submodels in atmospheric and climate models by remotely sensed *LAI* information has been found to improve the spatial variability of the atmospheric model response substantially [9]. Recently, it was suggested that land surface modelling would benefit significantly from improved characterization of the seasonal variability of vegetation at global scale [10]. A number of studies have demonstrated the potential of assimilating *LAI* observations to improve the vegetation description in land surface models and the implications of introducing the observed seasonal and interannual variability of *LAI* on the annual cycle of hydrological fluxes. In addition, using remotely sensed *LAI* in a model of global numerical weather prediction has been shown to improve the forecast of near-surface air temperature and relative humidity [11]. Although several *LAI* products based on remote sensing are available, the estimates may differ by up to 0.5 units in 80% of the pixels [12]. A recent thorough comparison of five major global *LAI* products indicated that their typical deviation is larger for forests (the difference being up to 1.0) than for other biomes. The *LAI* values differed more in summer than in winter. The largest observed differences occur in the boreal regions [12]. One reason for the difference could be the effect of the forest floor.

Global *LAI* estimation based on various satellite instruments relies in many cases on solving radiative transfer equations using some vegetation model [13, 14, 15]. The geometric-optical and kernel based approaches are motivated by their computation efficiency and easiness in investigating *BRDF*s for a large set of input parameters [16, 17, 18]. Commonly used kernels are the Ross-thick [19, 20], Ross-thin [19, 21], Roujean [20], Li-sparse [22] and Li-dense [23, 24]. These semi-empirical kernel models treat the land surface scattering as a sum of three components: isotropic, volume and geometric-optical scattering. The first component is related to the amount of the scattering material, the second component takes into account horizontally homogeneous leaf canopies and the third component pays attention to shadowing effects. The Ross-thin and Li-sparse kernels are used, for example, in generating the MODIS albedo product [24, 25].

For many forest types the forest floor vegetation is very scarce and the greenness can be attributed to the canopy only. In boreal forests, however, the forest floor vegetation is typically abundant and is actually used for classification of the boreal forest types [26]. Hence, the *BRF* model to be applied for boreal forests should also contain a component due to the forest floor. Spectral surface reflectance and related anisotropy descriptors can be used to provide this information, although they are typically tabulated for various soil types [13]. Improvements in

BRF description should also improve the canopy *LAI* estimates based on reflectance values retrieved using satellites. Actually, it is often easier to include the understory vegetation component in the model than getting the required input data for it. When fitting a *BRF* model to satellite data covering, for example, a time frame of one or two weeks, the forest floor component complicates the analysis whenever one cannot assume it to be constant within that time. In boreal forests this problem materializes (besides during winter time) especially at the beginning of the growing season, when the understory vegetation develops rapidly. Also blooming of the forest floor vegetation may complicate the analysis. Since the mean annual cloudiness of the boreal forest zone is typically in the order of 60% - 80% [27], it would be an advantage if the forest *BRF* model would not need many parameters to be fitted in order to be able to observe changes in the *LAI* value also at short time intervals.

In canopy reflectance models originating from the theory of spectral invariants [13, 28], the *BRF* of a vegetation canopy is derived as a function of the leaf single scattering albedo and three wavelength independent canopy structural parameters: canopy interceptance (i_0), the recollision probability (p) and the directional escape probability. In previous BRF models based on the spectral invariants theory [29, 30], the recollision probability has been assumed to be constant. In a recent study [31] this assumption was modified to allow the first order recollision probability (p_1) to be different from the multiple order recollision probability (p_d) (assumed to remain constant starting from the second interaction). Accordingly, the *BRF* of the first order scattering from the canopy (BRF_1) and the total *BRF* of the canopy were determined separately. Here the same approach is extended to include the forest floor contribution to the total *BRF* like in the PARAS forest albedo model [32]. The albedo model, however, only predicts the total hemispherical amount of radiation reflected by the canopy and the forest floor, not its angular variation as in the model presented here. The same modified spectral invariants approach is used for the forest floor as for the canopy. The new model is designed from the perspective of inversion of satellite images. The goal of this paper is to model and analyse the effect of the forest floor vegetation on the total forest *BRF*. We test the model using measured forest parameter values and satellite data. In addition, we compare the developed model with existing kernel-based models. The nomenclature related to the model is provided in Appendix A.

2. Theory and model description

2.1 BRF of the canopy

The recollision probability (p) is defined as the probability by which a photon scattered from a leaf or needle in the canopy will interact within the canopy again. Allowing the first recollision probability (p_1) to differ from the subsequent recollision probabilities (p_d), the canopy scattering coefficient (ω_C) takes the form [31]:

$$\omega_C = \omega_L(1-p_1) + \omega_L p_1 \frac{\omega_L}{1-p_d\omega_L}(1-p_d) \quad (1)$$

where ω_L is the leaf single scattering albedo.
Likewise, the bidirectional reflectance factor of the canopy at a given viewing space angle Ω, $BRF_c(\Omega)$, can then be expressed as the sum of the single and multiple order components [31, Eq. 15]

$$BRF_c(\Omega) = i_0\omega_L\rho_1(\Omega) + i_0\omega_L p_1 \frac{\omega_L}{1-p_d\omega_L}\rho_d(\Omega) = BRF_1(\Omega) + BRF_d(\Omega) \quad (2)$$

In Eq. (2), ρ_1 and ρ_d are the directional escape probabilities of the first order and the multiple order scattering, respectively. The canopy interceptance (i_0), in turn, is defined as the fraction of photons that enter the vegetation from above and are intercepted by elements in the canopy. It equals 1-P(Ω), where P is the mean value of the gap probability in the direction Ω over a horizontal plane beneath the canopy [31], and can be expressed as:

$$i_0 = 1 - \exp(-G\ LAI\ \beta/\cos\theta_i) \tag{3}$$

where *LAI* is the total leaf area index of the canopy, *G* is the mean projection of unit leaf (needle) area, β is the canopy clumping index and θ_i is the zenith angle of the incoming radiation. Woody elements are not explicitly included in the canopy description, but the *LAI* value used can actually be considered as the plant area index rather than the leaf area index. In the simulations (Section 1.1), β was assumed to be directionally independent [33] and for the coniferous canopies was given a constant value of 0.56. This value approximately accounts for the clumping of needles into shoots [34]. When applying the model to inversion of satellite reflectance values the standard deviation of neighbour high resolution pixels is an indicator of the applicability of the homogeneity assumption.

For simplicity we restrict ourselves to the case for which the reflectance and transmittance of the leaf are identical and thus equal to $\omega_L/2$. For coniferous boreal forests and some broadleaf species, the spherical leaf angle distribution (i.e. G = 0.5) has been shown to be a fair assumption [33, 35]. The bidirectional reflectance factor of the canopy from first scattering only is obtained as [31]:

$$BRF_1(\Omega) = \frac{1}{\cos\theta_i \cos\theta}\int_0^{LAI}\left(\frac{\omega_L}{3\pi}(\sin\gamma - \gamma\cos\gamma) + \frac{\tau}{3\cos\gamma}\right)\beta\ \exp(-G\ \beta\ y/\cos\theta_i)\beta\ \exp(-G\ \beta\ y/\cos\theta)dy \tag{4}$$

where ρ is the reflectance and τ is the transmittance of a leaf and the phase angle γ is defined by $\cos\gamma = \cos\theta_i\cos\theta + \sin\theta_i\sin\theta\cos\varphi$. Here θ and φ are the zenith and azimuth angles of the scattered radiation, choosing the azimuth angle of the incoming radiation to be zero. The azimuth angle is zero for the backscattering and π for the forward scattering direction. The bidirectional transmittance factor of the canopy in the space angle Ω of the first scattering in the canopy is obtained from

$$BTF_1(\Omega) = \frac{1}{\cos\theta_i \cos\theta}\int_0^{LAI}\left(\frac{\omega_L}{3\pi}(\sin\gamma - \gamma\cos\gamma) + \frac{\tau}{3\cos\gamma}\right)\beta\ \exp(-G\ \beta\ y/\cos\theta_i)\beta\ \exp(-G\ \beta\ (LAI - y)/\cos\theta)dy \tag{5}$$

Carrying out the integrations we obtain

$$BRF_1(\theta_i,\theta,\varphi,LAI,\beta,\omega_L) = \frac{\omega_L\beta\left(1-e^{-\frac{G(\cos\theta+\cos\theta_i)LAI\,\beta}{\cos\theta\cos\theta_i}}\right)}{6\,G\,\pi(\cos\theta+\cos\theta_i)}\Bigg(\Big(\pi - 2\cos^{-1}\left[\cos\theta\cos\theta_i+\sqrt{1-\cos\theta^2}\sqrt{1-\cos{\theta_i}^2}\cos\varphi\right]\Big)\Big(\cos\theta\cos\theta_i + \sqrt{1-\cos\theta^2}\sqrt{1-\cos{\theta_i}^2}\cos\varphi\Big) + 2\sqrt{1-(\cos\theta\cos\theta_i+\sqrt{1-\cos\theta^2}\sqrt{1-\cos{\theta_i}^2}\cos\varphi)^2}\Bigg) \quad (6)$$

$$BTF_1(\theta_i,\theta,\varphi,LAI,\beta,\omega_L) = \frac{\omega_L\beta\left(e^{-\frac{G\,LAI\,\beta}{\cos\theta}}-e^{-\frac{G\,LAI\,\beta}{\cos\theta_i}}\right)}{6\,G\,\pi(\cos\theta-\cos\theta_i)}\Bigg(\Big(\pi - 2\cos^{-1}\left[-\cos\theta\cos\theta_i+\sqrt{1-\cos\theta^2}\sqrt{1-\cos{\theta_i}^2}\cos\varphi\right]\Big)\Big(-\cos\theta\cos\theta_i + \sqrt{1-\cos\theta^2}\sqrt{1-\cos{\theta_i}^2}\cos\varphi\Big) + 2\sqrt{1-(\cos\theta\cos\theta_i-\sqrt{1-\cos\theta^2}\sqrt{1-\cos{\theta_i}^2}\cos\varphi)^2}\Bigg) \quad (7)$$

Both the denominator and numerator of BTF_1 approach zero when the viewing and sun zenith angles coincide, but the limit value of BTF_1 is finite and takes the form

$$BTF_1(\theta_i,\theta_i,\varphi,LAI,\beta,\omega_L) = \frac{\omega_L G\,LAI\beta^2 e^{-\frac{G\,LAI\,\beta}{\cos\theta_i}}}{6\,G\,\pi\cos^2\theta_i}\Big((\pi - 2\cos^{-1}[\cos{\theta_i}^2+\sin{\theta_i}^2\cos\varphi])(\cos{\theta_i}^2 + \sin{\theta_i}^2\cos\varphi) + 2\sqrt{1-(\cos{\theta_i}^2+\sin{\theta_i}^2\cos\varphi)^2}\Big) \quad . \quad (8)$$

The first order directional hemispherical reflectance (DHR_1) and directional hemispherical transmittance (DHT_1) of the canopy are

$$DHR_1(\theta_i,LAI,\beta,\omega_L) = \frac{1}{\pi}\int_0^{2\pi}\int_0^{\pi/2} BRF_1(\theta_i,\theta,\varphi,LAI,\beta,\omega_L)\cos\theta\sin\theta\,d\theta d\varphi \quad (9)$$

and

$$DHT_1(\theta_i,LAI,\beta,\omega_L) = \frac{1}{\pi}\int_0^{2\pi}\int_0^{\pi/2} BTF_1(\theta_i,\theta,\varphi,LAI,\beta,\omega_L)\cos\theta\sin\theta\,d\theta d\varphi \quad (10)$$

Unfortunately it is not possible to integrate Eqs. 9 and 10 in analytic form. Numerically derived analytic approximations for the DHR_1 and DHT_1 formulas are presented in the Appendix B. The first order recollision probability p_1 is related to DHR_1 and DHT_1 according to [31, Eq. 16]

$$p_1 = 1-\frac{DHR_1+DHT_1}{i_0\omega_L} = 1-\frac{DHR_1+DHT_1}{(1-e^{-0.5\,LAI\beta/\cos\theta_i})\omega_L} \quad (11)$$

The multiple order recollision probability p_d is related to LAI and the canopy diffuse interceptance i_D as [36]

$$p_d = 1 - \frac{i_D}{LAI} = 1 - \frac{1-e^{-0.5\,LAI\,\beta}(1-0.5\,LAI\,\beta)+(0.5\,LAI\,\beta)^2 Ei(-0.5\,LAI\,\beta)}{LAI} \quad (12)$$

where *Ei* is the exponential integral function Ei(z) = $-\int_{-z}^{\infty} e^{-t}/t\,dt$.

The bidirectional diffuse reflectance factor BRF_d (i.e. the second term of the right hand side of Eq. 2) is obtained from [31, Eq. 19]

$$BRF_d = \frac{1}{\pi}\frac{i_0 \omega p_1 \omega_L}{1-p_d\omega_L}\,\frac{1-\exp(-0.5\,LAI\,\beta)}{2\,LAI} \quad (13)$$

Combining Eqs. 11, 12 and 13 we get

$$BRF_d(\theta_i, LAI, \beta, \omega_L) = \frac{1}{\pi}\frac{0.5\omega_L\left(1-e^{-0.5LAI\,\beta}\right)\left(\omega_L\left(1-e^{-0.5\,LAI\,\beta/\cos\theta_i}\right)-DHR_1-DTH_1\right)}{LAI\left(1-\omega_L\left(1-\frac{4+2e^{-0.5LAI\beta}(LAI-2)+(LAI\,\beta)^2\,\mathrm{Ei}(-0.5LAI\,\beta)}{4\,LAI}\right)\right)} \quad (14)$$

and the total canopy BRF_c (with a black forest floor assumption and showing explicitly the angular, *LAI* and wavelength dependencies of Eq. 2) is

$$BRF_c(\theta_i, \theta, \varphi, LAI, \beta, \omega_L) = BRF_1(\theta_i, \theta, \varphi, LAI, \beta, \omega_L) + BRF_d(\theta_i LAI, \beta, \omega_L) \quad (15)$$

The diffuse fraction of the transmitted radiation is assumed to equal the diffuse fraction of the reflected radiation. Hence the total bidirectional transmission factor of the canopy is

$$BTF_c(\theta_i, \theta, \varphi, LAI, \beta, \omega_L) = BTF_1(\theta_i, \theta, \varphi, LAI, \beta, \omega_L) + BRF_d(\theta_i, LAI, \beta, \omega_L) \quad (16)$$

In boreal forests the forest floor is mostly vegetated, hence the *BRF* of the forest floor (without any canopy) in snow-free conditions (BRF_g) can be calculated similarly as the canopy BRF_c (Eq. 15). If the forest floor is snow covered, the forest floor *BRF* should be replaced by the *BRF* of snow. In principle, the photon recollision theory based approach may still be applied to generate the snow *BRF*, but then the phase function should permit also anisotropic scattering. *LAI* would be replaced by a parameter related to the surface area of the grains and β would be related to the complexity of the grain shape that causes multiple scattering from the same grain. For bare soil a similar generalization of the parameters can also be assumed.

2.2 Scattering components of direct radiation in the forest

The first scattering of radiation in the forest may take place either in the canopy or at the forest floor. For simplicity we show here only the angular dependence of the components of the total forest *BRF*, but the dependence on *LAI*, β and ω_L is like in the Eqs. 6 - 16 of section 2.1.

We first assume that the incoming radiation is completely directional with no diffuse component. Without violating generality we can take the azimuth angle of the incoming radiation to be $\varphi_i = 0$. There are four components of the radiation escaping from the canopy upwards in direction (θ_o, φ_o), where θ_o is the zenith angle and φ_o the azimuth angle of the outgoing radiation:

1. Scattering from the canopy only, BRF_{cc}
2. Scattering from the forest floor only, BRF_{gg}
3. Canopy and forest floor scattering with the last scattering originating from the canopy, BRF_{gc}
4. Canopy and forest floor scattering with last scattering from the floor, BRF_{cg}

The total forest *BRF* is then

$$BRF_f(\theta_i, \theta_o, \varphi_o) = BRF_{cc}(\theta_i, \theta_o, \varphi_o) + BRF_{gg}(\theta_i, \theta_o, \varphi_o) + BRF_{gc}(\theta_i, \theta_o, \varphi_o) + BRF_{cg}(\theta_i, \theta_o, \varphi_o) \quad (17)$$

The part of BRF_f originating from radiation scattered directly upwards from the canopy without ever reaching the forest floor (BRF_{cc}) coincides with the total canopy BRF assuming a black forest floor (BRF_c; Eq. 2):

$$BRF_{cc}(\theta_i, \theta_o, \varphi_o) = \frac{(1-t_0(\theta_i))BRF_c(\theta_i,\theta_o,\varphi_o)}{i_0(\theta_i)} = BRF_c(\theta_i, \theta_o, \varphi_o) \quad (18)$$

The fraction of radiation $t_0(\theta_i)$ reaching the forest floor without hitting the canopy (i.e. the uncollided canopy transmittance) is

$$t_0(\theta i) = \exp(-0.5\, LAI\, \beta / \cos\theta_i) \quad (19)$$

Likewise, the fraction of the radiation reflected from the forest floor and escaping the forest without hitting the canopy is $t_0(\theta_o)$. The fraction of radiation scattered at the forest floor in the case of no canopy is taken to be similar to the canopy scattering, so that it obeys Eqs. 1 and 19 with the forest floor vegetation parameters as input. Hence, the part of BRF_f originating from radiation scattered upwards by the forest floor without having interacted within the canopy is

$$BRF_{gg}(\theta_i, \theta_o, \varphi_o) = t_0(\theta_i) BRF_g(\theta_i, \theta_o, \varphi_o) t_0(\theta_o) \quad (20)$$

In Eq. (20) BRF_g is the reflectance factor of the forest floor vegetation and the two other components are the uncollided transmittances of the incident radiation and the radiation reflected from the forest floor, respectively.

The component BRF_{gc}, which has interacted with both the canopy and the forest floor, but has finally escaped from the canopy, can be described by introducing the directional distribution s_g (θ_i, θ_1, φ_1) of the radiation incident from zenith angle θ_i reaching the forest floor and being scattered (at first hit or after multiple scattering) from the forest floor to the canopy in the direction (θ_1, φ_1).

$$BRF_{gc}(\theta_i, \theta_o, \varphi_o) = \int_0^{2\pi} \int_0^{\pi/2} s_g(\theta_i, \theta_1, \varphi_1)\, BTF_c(\theta_1, \theta_o, \varphi_o - \varphi_1) / \big(1 - t_0(\theta_1)\big) \cos\theta_1 \sin\theta_1\, d\theta_1 d\varphi_1 \quad (21)$$

In the above formula, BTF_c is the bidirectional transmission factor of the canopy with black soil assumption (Eq. 16). Because scattering from the forest floor to the canopy may come from any direction, we have to integrate over all possible directions to get the total amount of radiation scattered from the forest floor to the canopy.
Similarly, the component BRF_{cg}, which has interacted with both the canopy and the forest floor, but has finally escaped from the forest floor, can be described by introducing the directional

distribution (s_d) of radiation scattered from the canopy to the forest floor. Like s_g it is defined as a function of the zenith angle of the incoming radiation and the zenith and azimuth angles of the scattered radiation:

$$BRF_{cg}(\theta_i, \theta_o, \varphi_o) = t_0(\theta_o) \int_0^{2\pi} \int_0^{\pi/2} s_d(\theta_i, \theta_1, \varphi_1) BRF_g(\theta_1, \theta_o, \varphi_o - \varphi_1) \cos\theta_1 \sin\theta_1 \, d\theta_1 d\varphi_1 \quad (22)$$

In the above formula, the radiation s_d scattered from the canopy to the forest floor (in all possible directions) is reflected by the forest floor vegetation (BRF_g) and then transmitted upwards through the canopy without hitting it (t_0). The two introduced scattering components s_d and s_g are related to each other by the following relationships

$$s_d(\theta_i, \theta_1, \varphi_1) = BTF_c(\theta_i, \theta_1, \varphi_1) + \int_0^{2\pi} \int_0^{\pi/2} s_g(\theta_i, \theta_2, \varphi_2) \, BRF_c(\theta_2, \theta_1, \varphi_1 - \varphi_2)/(1 - t_0(\theta_2)) \cos\theta_2 \sin\theta_2 \, d\theta_2 d\varphi_2 \quad (23)$$

$$s_g(\theta_i, \theta_2, \varphi_2) = t_0(\theta_i) BRF_g(\theta_i, \theta_2, \varphi_2)\big(1 - t_0(\theta_2)\big) + \big(1 - t_0(\theta_2)\big) \int_0^{2\pi} \int_0^{\pi/2} s_d(\theta_i, \theta_3, \varphi_3) BRF_g(\theta_3, \theta_2, \varphi_2 - \varphi_3) \cos\theta_3 \sin\theta_3 \, d\theta_3 d\varphi_3 \quad (24)$$

The first term of s_d describes the fraction of radiation that has first hit the canopy and then been scattered downwards to the forest floor. The second term describes the fraction of radiation that has been scattered from the forest floor to the canopy and then back to the forest floor. The first term of s_g describes the fraction of radiation that has first reached the forest floor without hitting the canopy, then been scattered upwards by the forest floor vegetation and avoided escaping from the forest by hitting the canopy. The second term describes the fraction of radiation that has been scattered downwards from the canopy to the forest floor, then scattered by the forest floor vegetation and then instead of escaping from the forest hit the canopy to continue scattering (or absorption) there. BRF_c describes the amount reflected to the same hemisphere where the radiation came from. BTF_c describes the amount reflected to the hemisphere opposite to the one where the radiation came from. In the above equations it is assumed that BRF_c and BTF_c do not depend on whether the radiation is entering the canopy from above or below. The assumption is justified by the definitions of BRF_c and BTF_c, which do not include any information about the canopy direction (i.e. whether the trees are upside down or not). The explicit formulas for s_d and s_g are derived in Appendix C.

Substituting Eqs. B6 and B7 into Eqs. 21 and 22 we get the total forest *BRF* (Eq. 17). Unfortunately the latter two components of the forest scattering (Eqs. 21 and 22) involve multiple integrals of so complicated combinations of the basic *BRFs* and *BTFs* that using approximate functions in the integrands will not produce very accurate results. Thus, numerical integration and interpolation are used in calculating BRF_f.

The spectral directional hemispherical reflectance of the forest, i.e. the black-sky albedo (DHR_f), is then obtained by integrating Eq. 17 over all reflection directions

$$DHR_f(\theta_i) = \frac{1}{\pi} \int_0^{\pi/2} \int_0^{2\pi} BRF_f(\theta_i, \theta_o, \varphi_o) \cos\theta_o \sin\theta_o \, d\varphi_o d\theta_o \quad (25)$$

The four components of the spectral black-sky albedo are likewise obtained by integration of Eqs. 18, 20 - 22.

2.3 Scattering components of diffuse radiation in the forest

When the incoming radiation is completely diffuse, the fraction of radiation scattered from the forest to direction (θ_o, φ_o), $HDRF_f$, (θ_o, φ_o), is obtained by integrating the BRF_f over the angles of the incoming radiation (θ_i, φ_i) [37]. The four components of $HDRF_f$ are:
1. Scattering from the canopy only, $HDRF_{cc}$
2. Scattering from the forest floor only, $HDRF_{gg}$
3. Canopy and forest floor scattering with last scattering from the canopy, $HDRF_{gc}$
4. Canopy and forest floor scattering with last scattering from the forest floor, $HDRF_{cg}$

The total fraction of the diffuse radiation scattered into direction (θ_o, φ_o) is:

$$HDRF_f(\theta_o, \varphi_o) = HDRF_{cc}(\theta_o, \varphi_o) + HDRF_{gg}(\theta_o, \varphi_o) + HDRF_{gc}(\theta_o, \varphi_o) + HDRF_{cg}(\theta_o, \varphi_o) \quad (26)$$

The spectral bi-hemispherical reflectance of the forest, i.e. the white-sky albedo, (BHR_f), is then obtained by integrating Eq. 26 over all reflection directions.

$$BHR_f = \frac{1}{\pi}\int_0^{2\pi}\int_0^{\pi/2} HDRF_f(\theta_o, \varphi_o)\cos\theta_o \sin\theta_o d\theta_o\, d\varphi_o \quad . \quad (27)$$

Typically the global irradiance consists of direct and diffuse components. Then the fraction of the incoming radiation per unit area scattered in direction (θ_o, φ_o) can be expressed as

$$BHDRF_f(\theta_i, \theta_o, \varphi_o) = BRF_f(\theta_i, \theta_o, \varphi_o)(1 - D) + HDRF_f(\theta_o, \varphi_o)\, D \quad (28)$$

where D is the fraction of the diffuse irradiance. Likewise the blue-sky albedo ($DBHR_f$) is

$$DBHR_f(\theta_i) = DHR_f(\theta_i)(1 - D) + BHR_f D \quad (29)$$

2.4 Hotspot effect

In the previous analysis the hotspot effect was not taken into account. A simple approximation for it is to multiply BRF_1 with the hotspot term, like in [38, 39]. Then Eq. 6 is replaced by

$$\begin{aligned} BRF_1'(\theta_i, \theta, \varphi, LAI, \beta, \omega_L) &= \left(1 + c_1 e^{c_2|\theta - \theta_i|/\pi}\right) \frac{\omega_L \beta \left(1 - e^{-\frac{(\cos\theta + \cos\theta_i) LAI\, \beta}{2\cos\theta\cos\theta_i}}\right)}{3\pi(\cos\theta + \cos\theta_i)} \Bigg(\Big(\pi \\ &- 2\cos^{-1}\left[\cos\theta\cos\theta_i + \sqrt{1 - \cos\theta^2}\sqrt{1 - \cos\theta_i{}^2}\cos\varphi\right]\Big)\left(\cos\theta\cos\theta_i \right. \\ &\left. + \sqrt{1 - \cos\theta^2}\sqrt{1 - \cos\theta_i{}^2}\cos\varphi\right) \\ &+ 2\sqrt{1 - (\cos\theta\cos\theta_i + \sqrt{1 - \cos\theta^2}\sqrt{1 - \cos\theta_i{}^2}\cos\varphi)^2} \Bigg) \end{aligned} \quad (30)$$

where c_1 and c_2 are hotspot coefficients related to the canopy properties [39].

Now more energy is reflected to the incoming direction than when using Eq. 6 for BRF_1 and subsequently this energy must be removed from other components, namely BTF_1 and BRF_d. To conserve energy, the sum of the diverse energy components (Eqs. 15 and 16) must equal unity, i.e.

$$\frac{1}{\pi}\int_0^{2\pi}\int_0^{\frac{\pi}{2}} BRF_1(\theta_i,\theta,\varphi,LAI,\beta,\omega_L)\cos\theta\sin\theta\, d\theta d\varphi + \frac{1}{\pi}\int_0^{2\pi}\int_0^{\frac{\pi}{2}} BTF_1(\theta_i,\theta,\varphi,LAI,\beta,\omega_L)\cos\theta\sin\theta\, d\theta\, d\varphi + 2\, BRF_d(\theta_i) = 1 \tag{31}$$

When the extra amount of reflected radiation due to the hotspot effect is subtracted from the other terms by an equal fraction k depending on the cosine of the zenith angle of the incident radiation, we get

$$\frac{1}{\pi}\int_0^{2\pi}\int_0^{\frac{\pi}{2}} BRF_1'(\theta_i,\theta,\varphi,LAI,\beta,\omega_L)\cos\theta\sin\theta\, d\theta\, d\varphi + k(\cos\theta_i)\frac{1}{\pi}\int_0^{2\pi}\int_0^{\frac{\pi}{2}} BTF_1(\theta_i,\theta,\varphi,LAI,\beta,\omega_L)\cos\theta\sin\theta\, d\theta d\varphi + 2\, k(\cos\theta_i)BRF_d(\theta_i) = 1 \tag{32}$$

The coefficient k can now be solved from the above two equations and we get

$$k(\cos\theta_i) = 1 - \frac{\int_0^{2\pi}\int_0^{\frac{\pi}{2}}\left(BRF_1'(\theta_i,\theta,\varphi) - BRF_1(\theta_i,\theta,\varphi)\right)\cos\theta\sin\theta\, d\theta\, d\varphi}{\int_0^{2\pi}\int_0^{\frac{\pi}{2}} BTF_1(\theta_i,\theta,\varphi,LAI,\beta,\omega_L)\cos\theta\sin\theta\, d\theta\, d\varphi + 2\, BRF_d(\theta_i)} \tag{33}$$

Now BTF_1 and BRF_d of Eqs. 15 and 16 are replaced by $k(\cos\theta_i)$ times BTF_1 and BRF_d in further analysis. The numerical approximations of the *DHR* and *DHT* (Appendix B) are not applicable for the hotspot case and deriving numerical approximations for BRF_1 and BTF_1 is beyond the scope of this study.

In principle a similar hotspot effect also concerns the forest floor vegetation in Eq. 20, but typically it would be even smaller than that of the canopy.

3. Results

3.1 Comparison with kernel based BRF estimates

Kernel based *BRF* models are usually formulated so that the reflectance R consists of three components [19, 20, 21, 22, 23, 24]

$$R = f_{iso} + f_{geo}k_{geo} + f_{vol}k_{vol} \quad (34)$$

where k_{geo} and k_{vol} are the geometric and volumetric kernels and f_{iso}, f_{geo} and f_{vol} are parameters related to the canopy characteristics, such as *LAI*. In the kernels by Ross [19] and Roujean et al. [20], the angular dependency of k_{geo} and k_{vol} is separated from the canopy characteristics dependency. For the Li-sparse and Li-dense kernels [21, 22, 23, 24], the angular variation of *BRF* depends also on the vertical and horizontal dimensions ($2b$ and $2r$, respectively) of the crown and the distance h to the centre of the crown above the ground.

Example cases are calculated using the Ross-thick, Ross-thin, Roujean, Li-sparse and Li-dense kernels [**Error! Reference source not found.**]. The hotspot effect manifested by the geometric Roujean and Li kernels is not included in the new *BRF* model simulations, but the formalism for taking it into account is presented in Section 2.4. Therefore those kernels differ essentially from our model results, which seem to resemble the volumetric kernels by Ross and Roujean. The developed *BRF* model [Figure 2] cannot either be directly compared to the Roujean and Li kernels, because the present *BRF* model depends on *LAI*, β and ω_L for the canopy and forest floor separately, whereas those kernels depend on parameters related to the canopy crown properties. Hence, the model is calculated for some example *LAI*, β and ω_L combinations of the canopy and forest floor [Table 1] to show the qualitative effect on the angular variation of the *BRF*. In addition, the model *BRF* is compared to the Ross kernels [Figure 2].

It turned out that the correlation with the modelled *BRF* and the Ross-thick kernel is good for all studied cases, the R^2 value varying in the range 0.88… 0.99997 (for 18 point fits). The R^2 is higher for the sun zenith angle of 60º than of 30º, and for the canopy *LAI* value of 4 than 1. The effect of the forest floor vegetation *LAI* is minor (especially when the view zenith angle is smaller), but slightly higher R^2 values correspond to the dense than to the sparse forest floor vegetation. The good agreement with the Ross-thick kernel is in line with the good results obtained when using the Ross-thick kernel for estimating the angular variation of reflectance due to volumetric canopy scattering, like in the MODIS albedo product retrieval [24, 25]. Only

Table 1. The parameter values used in simulations of forest and canopy *BRF*.

Parameter	Value	Reference
Sun zenith angle	30°, 60°	
View zenith angle	0°, 10°, 20°, 30°, 40°, 50°, 60°, 70°, 80°	
Azimuth angle	0°, 180°	
Canopy clumping index β	0.56	[41]
Understory vegetation clumping index β_g	1	-
Canopy leaf single scattering albedo $\omega_{L,}$ Red	0.1	[49]
Canopy leaf single scattering albedo $\omega_{L,}$ NIR	0.7	[49]
Forest floor vegetation leaf single scattering albedo ω_L, Red	0.07	[50]
Forest floor vegetation leaf single scattering albedo $\omega_{L,}$ NIR	0.3	[50]
Dense forest *LAI*	4	
Sparse forest *LAI*	1	
Dense forest floor vegetation	4	
Sparse forest floor vegetation	1	

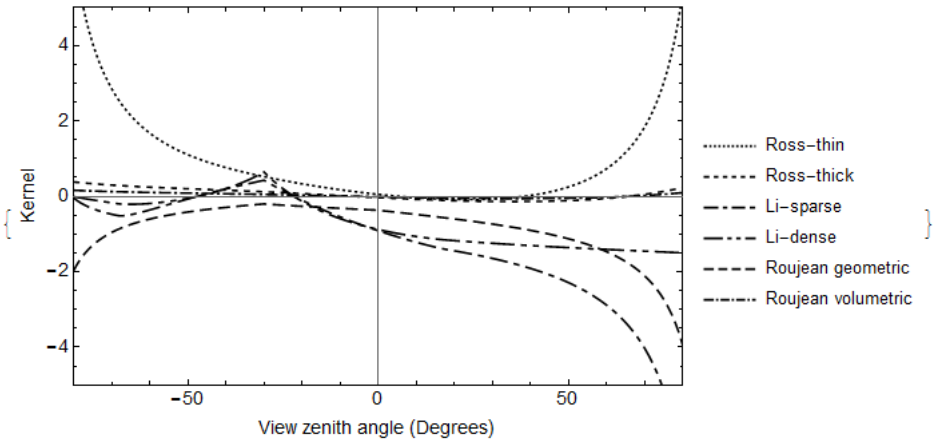

a)

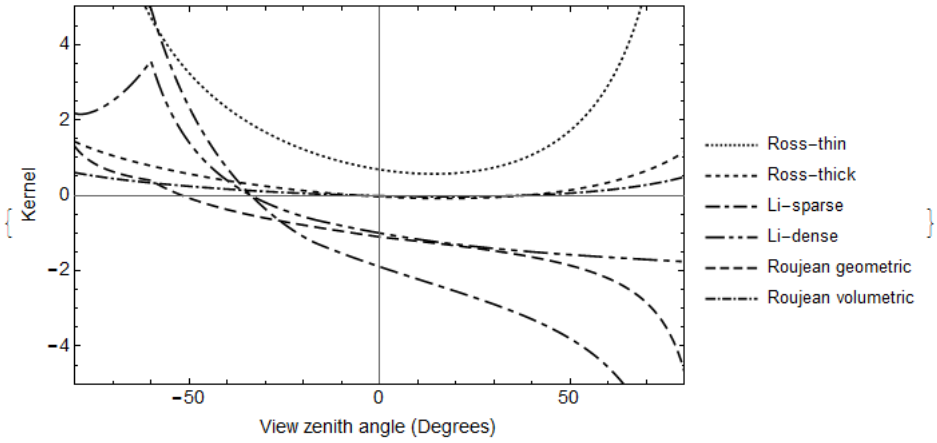

b)

Figure 1. Commonly used kernels for the sun zenith angle values a) 30° and b) 60° [19, 20, 21, 22, 23]. For the Li kernels the values h/b = 1.8 and b/r = 2.5 were used, because they were close to typical values measured in boreal forest in Finland [40]. Positive (negative) values of the view zenith angle correspond to forward (backward) scattering.

when the forest is sparse, the relationship between BRF_f and the Ross-thick kernel is somewhat weaker. However, the regression coefficients do not have a clear dependence on the canopy *LAI*. Hence, reliable *LAI* estimation is not possible with the Ross-thick kernel in cases where the forest floor reflectance is not negligible. When the given dependence of the Ross-thick kernel coefficients on *LAI* [21] is applied to the regression coefficients of the modelled BRF_f vs. the Ross-thick-kernel to derive the canopy *LAI*, the results are far from the *LAI* values used as input for the modelled BRF_f. The zero order coefficient may even be negative [Figure 2], which would result in a negative forest floor reflectance or leaf single scattering albedo. For the *LAI* values used in the kernel simulations, the mean relative difference between the true *LAI* values and the values obtained from the linear regression is 77% for the red wavelength range and 46% for the NIR wavelength range. The estimates for the *LAI* values of 4 are not any better than those for the *LAI* value 1.

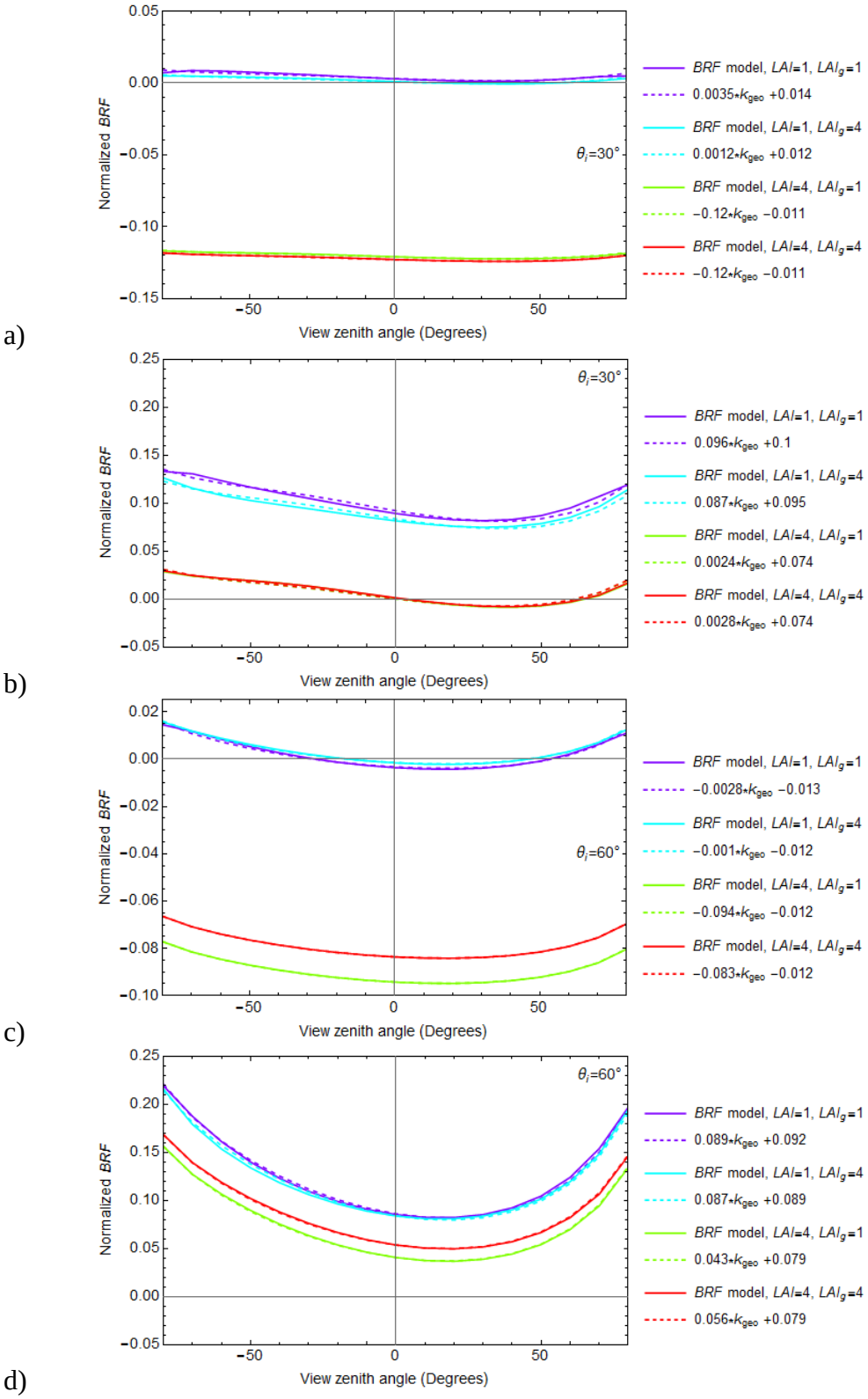

Figure 2. Relative variation of the reflectance values in the principal plane derived using the developed *BRF* model for the sun zenith angle value 30° and a) red and b) NIR channels and for the sun zenith angle value 60° and c) red and d) NIR channels. The corresponding nadir reflectance value has been subtracted from the modelled *BRF* curves. Positive (negative) values of the view zenith angle correspond to forward (backward) scattering.

3.2 Comparison with measurements

The capability of the model to simulate measurements is tested using a data set [Table 2] measured at the Hirsikangas LAI site in central Finland. A detailed site and measurement description can be found in [40]. This data set exceptionally contains both the canopy and combined canopy and forest floor vegetation *LAI*, which then provides a direct estimate for the forest floor vegetation *LAI*. One SPOT image of August 2, 2003 is also available. For comparison with the model results, the SPOT image reflectance values are averaged in a 3 x 3 window. The sun and satellite angle values used in the simulations correspond to this SPOT image [Table 3]. Values of the leaf single scattering albedo and the clumping index for the canopy and the understory vegetation are obtained from existing measurement data of similar forest sites. The former ones are provided separately for sun exposed and shaded needles or leaves [Table 4].

Table 2. The test *LAI* data set measured at Hirsikangas in 2003 [40]. Most of the 30 stands were pure pine stands, five mixed and one pure spruce and two pure birch stands.

	Minimum	Average	Maximum
Latitude (º)	62.6318	62.6435	62.6575
Longitude (º)	26.9846	27.0095	27.0335
Altitude a.s.l. (m)	103	119	147.3520
Canopy LAI	0.27	2.18	4.52
Forest floor LAI	0.43	2.83	5.52

Table 3. The sun and satellite angles corresponding to the SPOT image of August 2, 2003 of Hirsikangas.

Sun zenith angle (º)	45.45
Sun azimuth angle (º)	165.55
Satellite zenith angle (º)	13.8
Satellite azimuth angle (º)	257.82

Table 4. The parameter values used in calculations of the Hirsikangas *BRF* [38, 48, 49].

Parameter				Value	Reference
Canopy clumping index β				0.56	[41]
Understory vegetation clumping index β_g				1	-
Leaf single scattering albedo ω_L	Scots pine	Red	Sun exposed	0.3	[48]
			shaded	0.2	[48]
		NIR	sun exposed	0.9	[48]
			shaded	0.85	[48]
	Norway spruce	Red	sun exposed	0.22	[48]
			shaded	0.2	[48]
		NIR	sun exposed	0.83	[48]
			shaded	0.79	[48]
	Silver birch	Red	sun exposed	0.23	[48]
			shaded	0.24	[48]
		NIR	sun exposed	0.95	[48]
			shaded	0.95	[48]

The modelled BRF_f and BRF_c values are very sensitive to the choice of the leaf single scattering albedo (ω_L). When values corresponding to sun exposed needles or leaves are used as input, BRF_f both in the red and NIR channels are on the average -0.005 lower than the corresponding SPOT channel reflectance values (when the reflectance value is given in the range 0…1). For BRF_c, the corresponding deviation is -0.009 in the red channel and -0.04 in the NIR channel. When values corresponding to shaded needles or leaves are used, the deviation from the satellite based reflectance values is in the red channel 0.0004 for BRF_c and 0.01 for the BRF_f. In the NIR channel, the corresponding deviation is -0.01 for BRF_c and 0.03 for BRF_f. An optimal choice for the leaf single scattering albedo would probably thus be something between the sun exposed and shaded needles or leaves, which seems quite realistic. For the shaded needles or leaves, the mean difference between the forest and canopy *NDVI* values is 2 % and the mean difference between the forest and canopy *SR* values is 8 %. For the sun exposed needles or leaves the corresponding values are 0.3 % and 2.3 %, respectively.

The modelled *NDVI* values for the forest correlate better than those of the canopy with the *NDVI* values obtained from the SPOT image [Figure 3]. The model results obtained using ω_L corresponding to shaded needles or leaves are closer to the corresponding SPOT image based values than those using ω_L for the sun exposed needles or leaves. The average difference of the model and satellite based *NDVI* values is 0.03 for the sun exposed case and -0.003 for the shaded case with a standard deviation of 0.04 and 0.03, respectively. Because the forest floor vegetation is assumed to have the same optical properties (measured for coniferous forests) for all stands, it is understandable that the points that deviate most strongly from the SPOT based *NDVI* values are a pure birch stand and a pure pine stand having an *LAI* value of only 0.27. Some scatter is probably caused also by the forest floor vegetation *LAI* values, which do not take into account the possible moss or lichen layer on the forest floor.

1.1 Simulated reflectance values and vegetation indices

The effect of the forest floor on the total forest BRF_f, and on the values of *SR* and *NDVI*, is demonstrated for some cases typical of boreal forest. The simulations are made for sparse and dense forests and forest floor vegetations, two wavelength ranges (red and NIR), and for varying view zenith angles in the principal plane [Table 1]. The sun zenith angle value 60º is typical in the boreal zone for long periods (spring, autumn). The ω_L values chosen are smaller than the measured values in Table 4, in order to study the forest floor effect of a case for which the effect should not be overly pronounced. The clumping index is chosen to account for shoot scale clumping in boreal coniferous forests.

Variation of the forest and canopy *BRFs* with the view zenith angle are shown for sparse and dense canopies and forest floor vegetation in Figure 4 - Figure 7. The results are presented for the sun zenith angle values of 30° and 60° and for the red and NIR wavelength ranges. The largest effect of the forest floor vegetation on the total forest *BRF* naturally occurs when the canopy is sparse and the sun zenith angle value is small. The effect decreases with increasing view zenith angle. For the sparse canopy, the relative difference of the canopy and forest *BRFs* is larger for the red wavelength range than for the NIR wavelength. For the dense canopy, the phenomenon is the opposite: the effect is stronger in the NIR than in the red wavelength range. For the larger sun zenith angle value and the denser canopy, the forest floor does not have a noticeable effect in the red wavelength range, but in the NIR wavelength range the effect is still non-negligible.

Although the relative forest floor contribution to the total forest *BRF* is largest for a nadir view, it does not change markedly within the view zenith angle range 0º - 60º, which is the typical view angle range used for satellite images [Table 5]. For sparse forest, 39 % - 69 % of the red channel reflectance and 34 % - 54 % of the NIR channel reflectance may come from the forest floor vegetation, depending on the sun and view zenith angle values. For dense forests, the corresponding forest floor contribution varies between 2 % and 16 % for the red channel, and between 7 % and 18 % for the NIR channel. It does not matter much whether the forest floor vegetation *LAI* is dense or sparse.

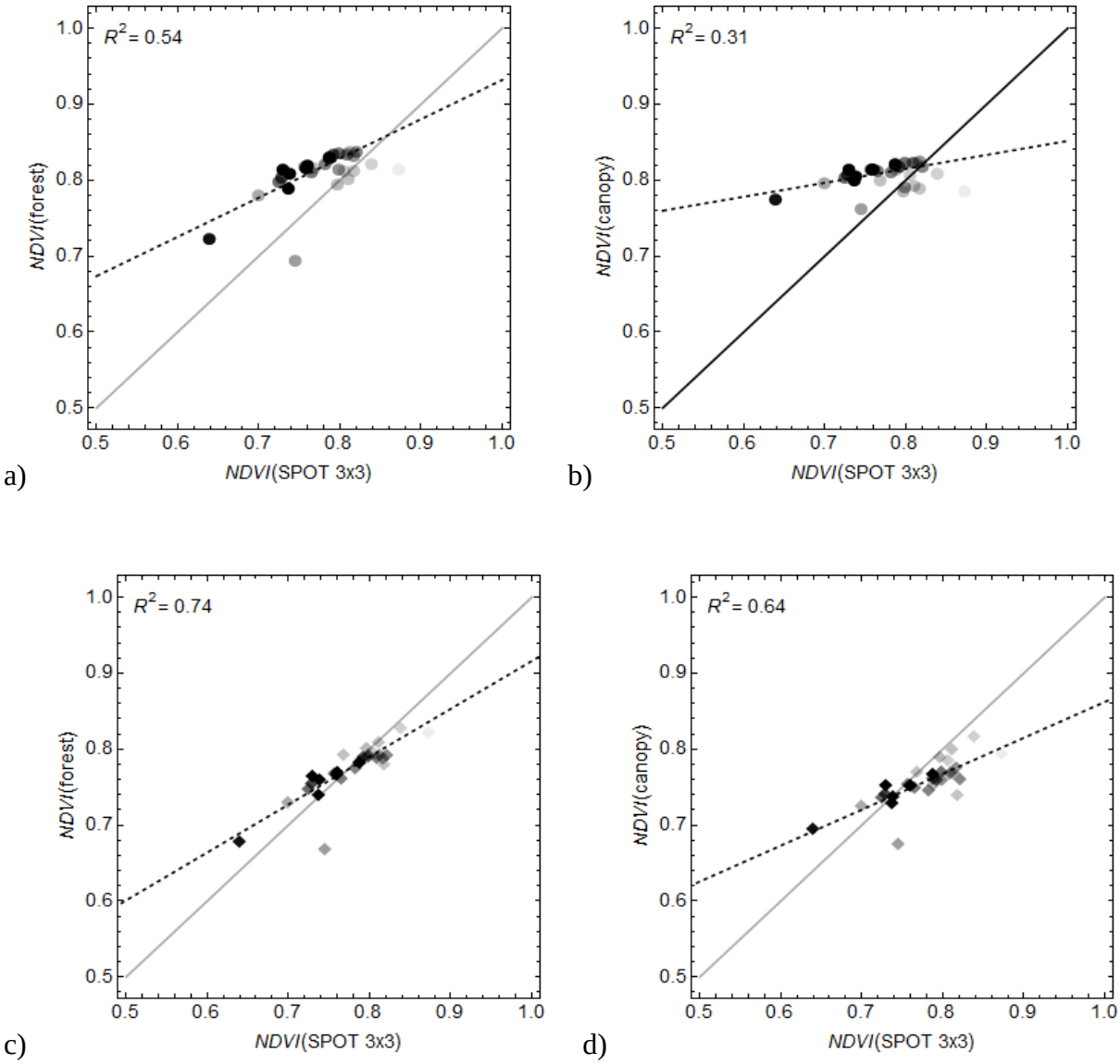

Figure 3. The modelled *NDVI* value of the forest (a & c) and the canopy (b & d) compared to the *NDVI* value derived in a 3x3 window of the SPOT image for the Hirsikangas site. The circles (a & b) represent model results using the albedo values of sun exposed needles or leaves and the diamonds (c & d) represent those for shaded needles or leaves. The opacity of the points is proportional to the inverse of the standard deviation of 3x3 window pixel values in the NIR channel of the SPOT image.

Table 5. Relative contribution of the forest *BRF* in the red and NIR wavelength range caused by the forest floor vegetation for various values of *LAI*, LAI_g, θ_i, φ and θ_o.

Wavelength range	θ_i	φ	*LAI*	LAI_g	$(BRF_f - BRF_c)/BRF_f$		
					$\theta_o = 0^o$	$\theta_o = 60^o$	$\theta_o = 80^o$
Red	30º	180º	1	1	0.69	0.62	0.33
			1	4	0.63	0.51	0.22
			4	1	0.16	0.07	0.005
			4	4	0.13	0.05	0.005
		0º	1	1	0.69	0.62	0.33
			1	4	0.63	0.50	0.21
			4	1	0.16	0.07	0.004
			4	4	0.13	0.05	0.005
	60º	180º	1	1	0.55	0.46	0.21
			1	4	0.50	0.40	0.16
			4	1	0.06	0.02	0.001
			4	4	0.05	0.02	0.002
		0º	1	1	0.55	0.46	0.21
			1	4	0.50	0.39	0.16
			4	1	0.06	0.02	0.001
			4	4	0.05	0.02	0.001
NIR	30º	180º	1	1	0.54	0.50	0.31
			1	4	0.50	0.44	0.28
			4	1	0.16	0.12	0.06
			4	4	0.18	0.13	0.08
		0º	1	1	0.54	0.50	0.30
			1	4	0.50	0.43	0.27
			4	1	0.16	0.11	0.06
			4	4	0.18	0.12	0.07
	60º	180º	1	1	0.44	0.40	0.22
			1	4	0.41	0.36	0.20
			4	1	0.12	0.08	0.04
			4	4	0.13	0.09	0.04
		0º	1	1	0.44	0.38	0.22
			1	4	0.41	0.34	0.19
			4	1	0.12	0.07	0.03
			4	4	0.13	0.07	0.04

The comparison of the *SR* and *NDVI* values computed from BRF_c and BRF_f are shown in Figure 8 and Figure 9. Obviously, the difference between the *SR* values of the canopy and the forest increases with decreasing canopy *LAI*. The effect of the forest floor on *SR* and *NDVI* can be either positive or negative. For the simulated data, the relative difference of the forest and canopy *SR* values is in the range -19% to 9% for the sun zenith angle value 60º, and -33% to 10% for the sun zenith angle value 30º. For *NDVI*, the corresponding range for the relative difference is -5% to 1% for the sun zenith angle value 60º, and -9% to 2% for the sun zenith angle value 30º. When *LAI* is estimated using vegetation indices, the relationship is typically assumed to be linear. Then relative error of the *SR* and *NDVI* also represents the relative error of the *LAI* estimates based on these indices.

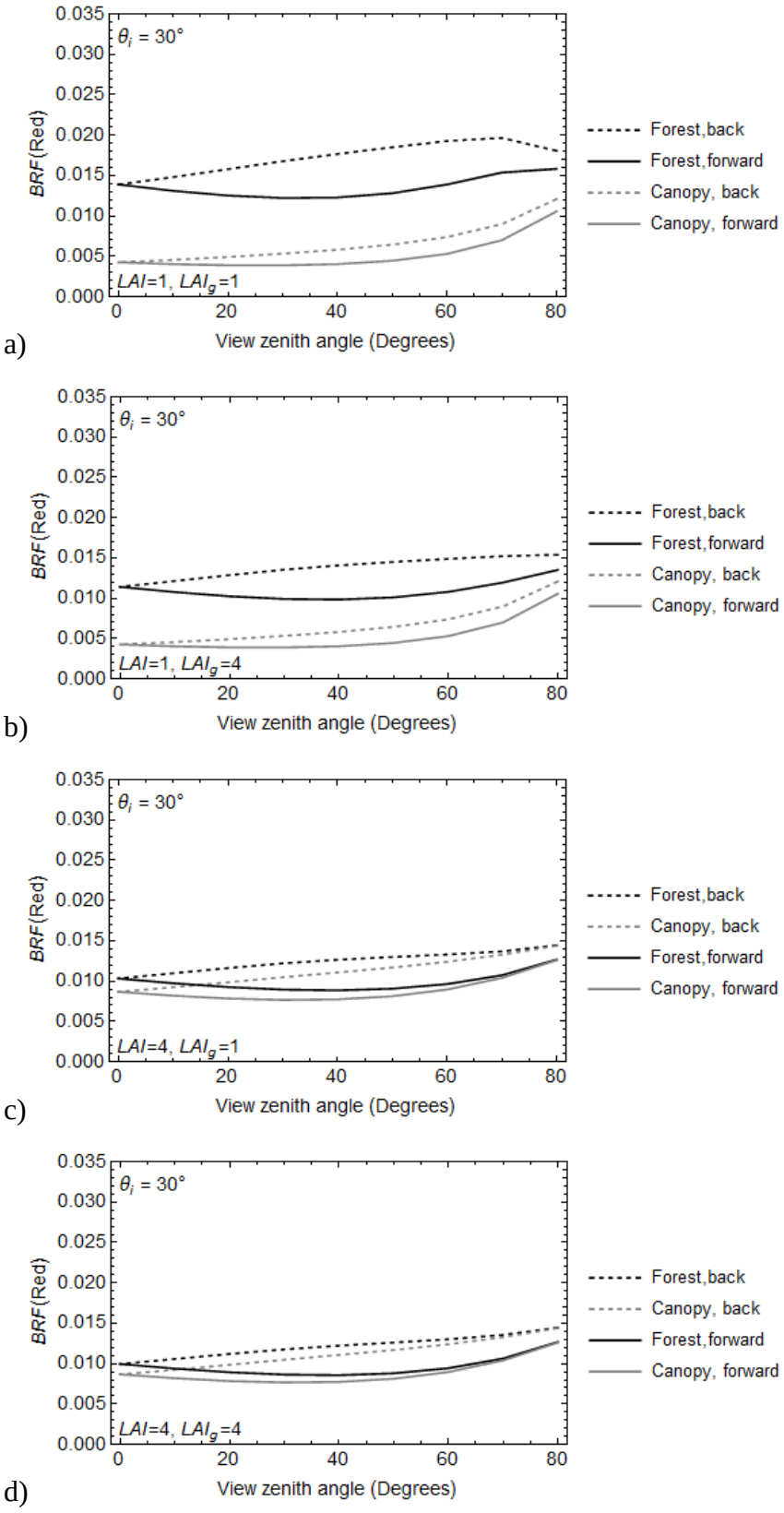

Figure 4. Variation of the canopy and forest *BRFs* in the red wavelength range with the view zenith angle for the sun zenith angle value 30° in the principal plane for various *LAI* values of the canopy and forest floor vegetation.

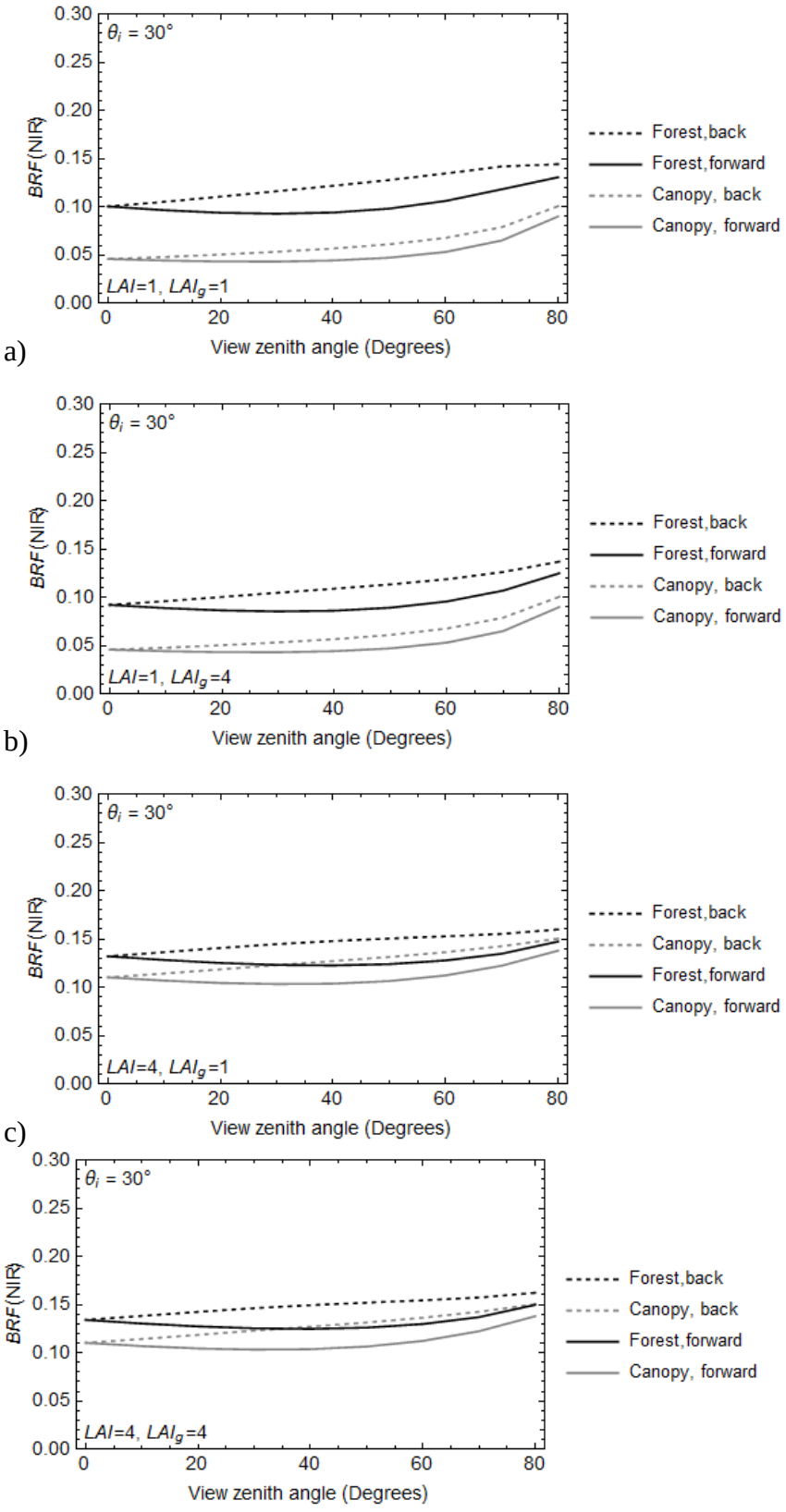

Figure 5. Variation of the canopy and forest *BRFs* in the NIR wavelength range with the view zenith angle for the sun zenith angle value 30° in the principal plane for various *LAI* values of the canopy and forest floor vegetation.

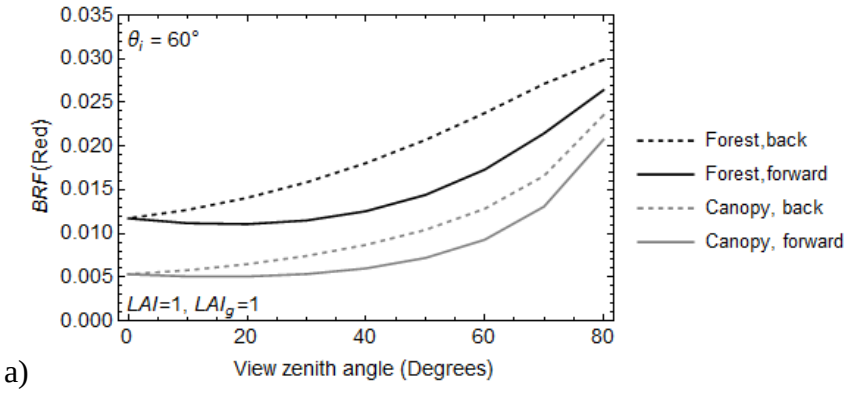

a)

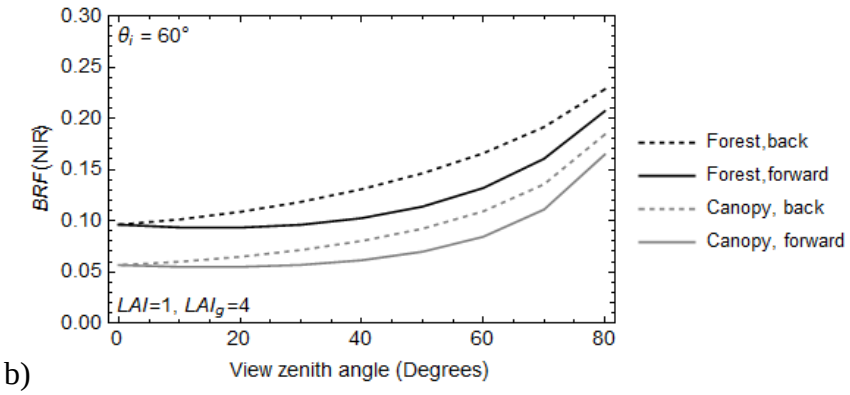

b)

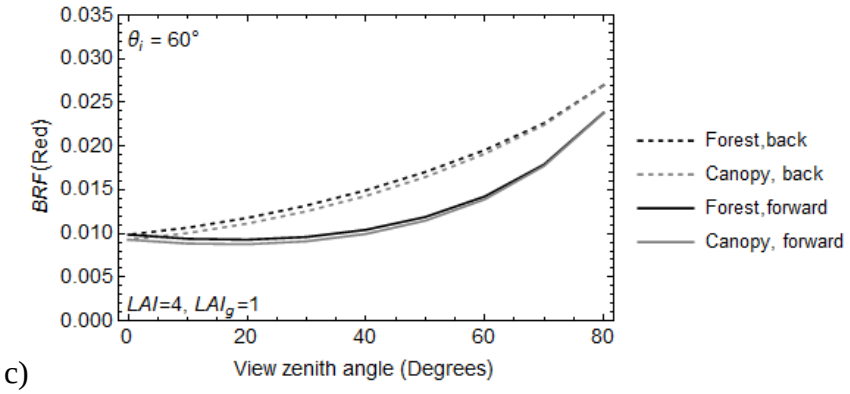

c)

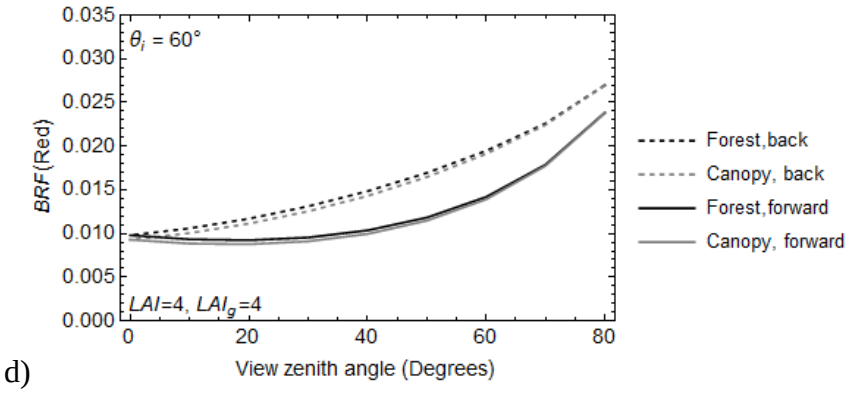

d)

Figure 6. Variation of the canopy and forest *BRFs* in the red wavelength range with the view zenith angle for the sun zenith angle value 60° in the principal plane for various *LAI* values of the canopy and forest floor vegetation.

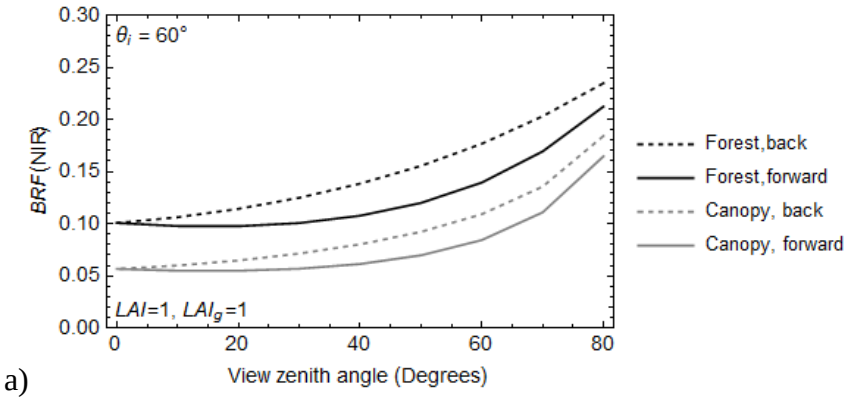

a)

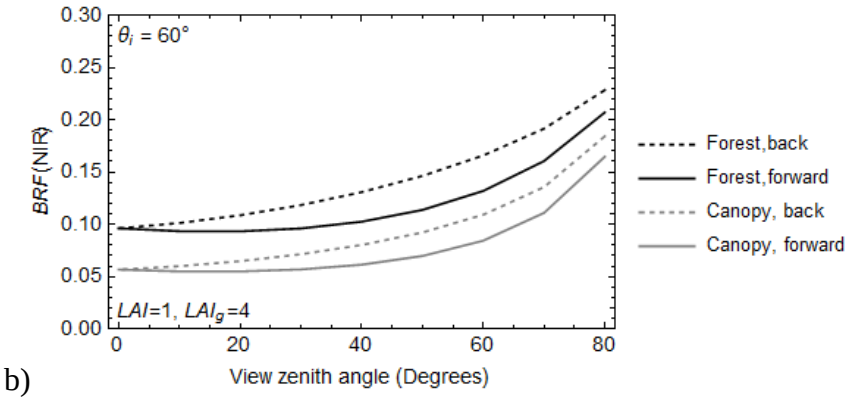

b)

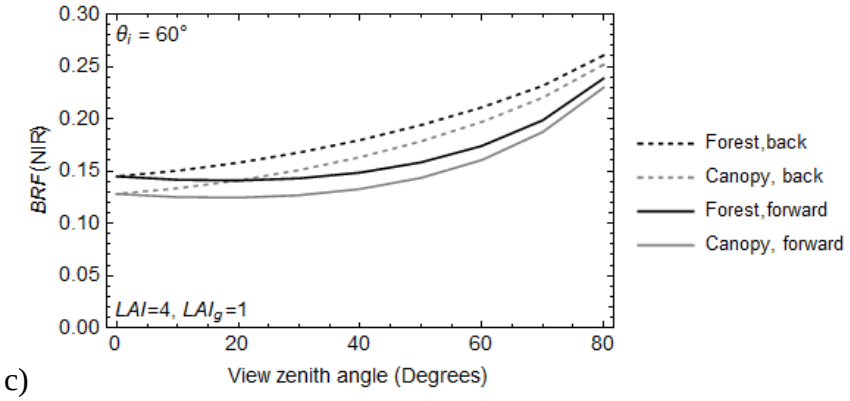

c)

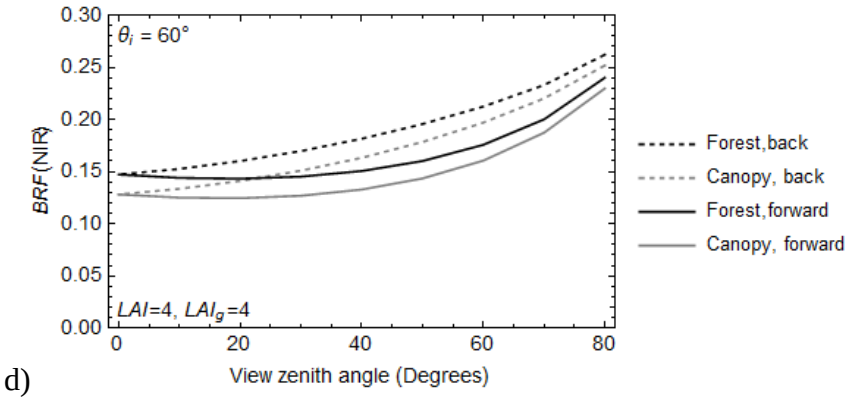

d)

Figure 7. Variation of the canopy and forest *BRFs* in the NIR wavelength range with the view zenith angle for the sun zenith angle value 60° in the principal plane for various *LAI* values of the canopy and forest floor vegetation.

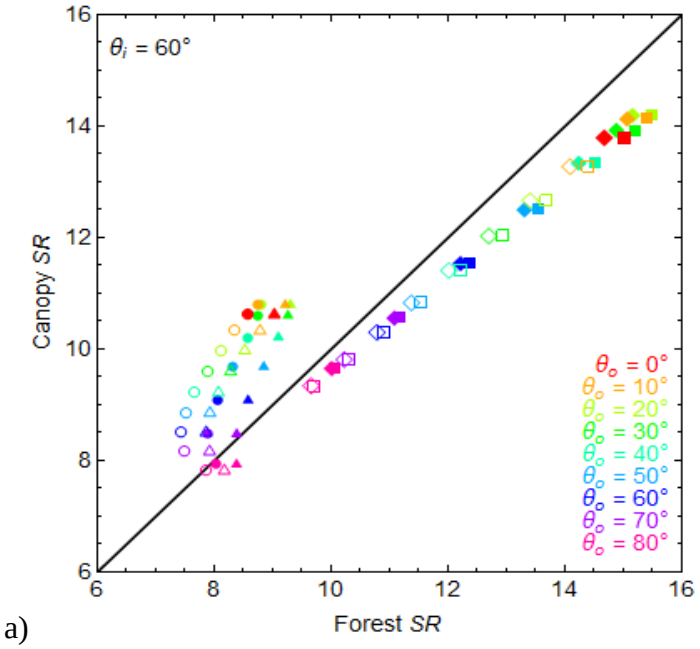

a)

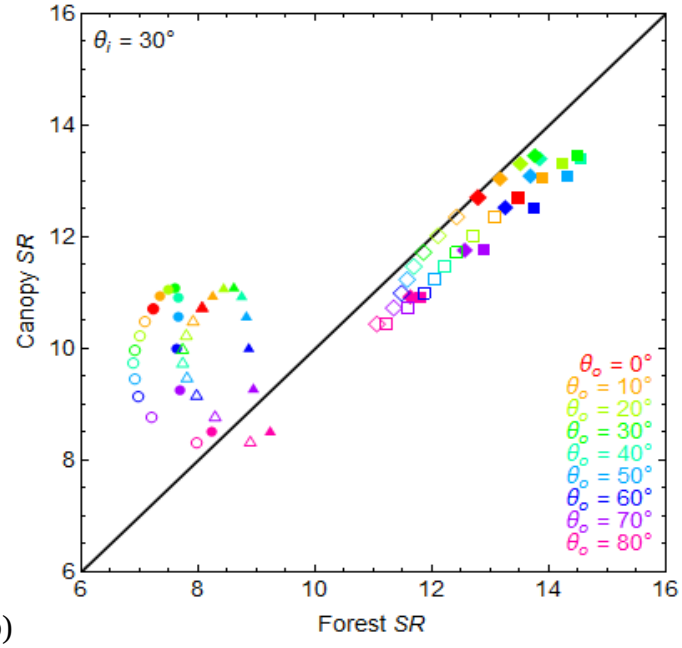

b)

Figure 8. The *SR* value of the canopy as a function of the forest *SR* value for various values of view zenith angle and the sun zenith angle values 60º (a) and 30º (b). The solid symbols indicate the forward scattering direction and the open symbols the backscattering direction. The markers denote: circles: (*LAI* = 1, LAI_g =1), triangles: (*LAI* = 1, LAI_g = 4), diamonds: (*LAI* = 4, LAI_g = 1), and squares: (*LAI* = 4, LAI_g = 4).

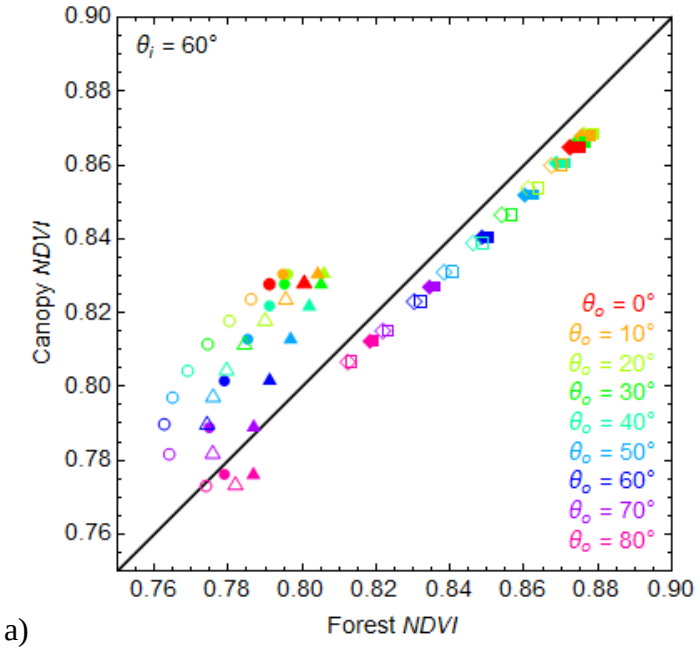

a)

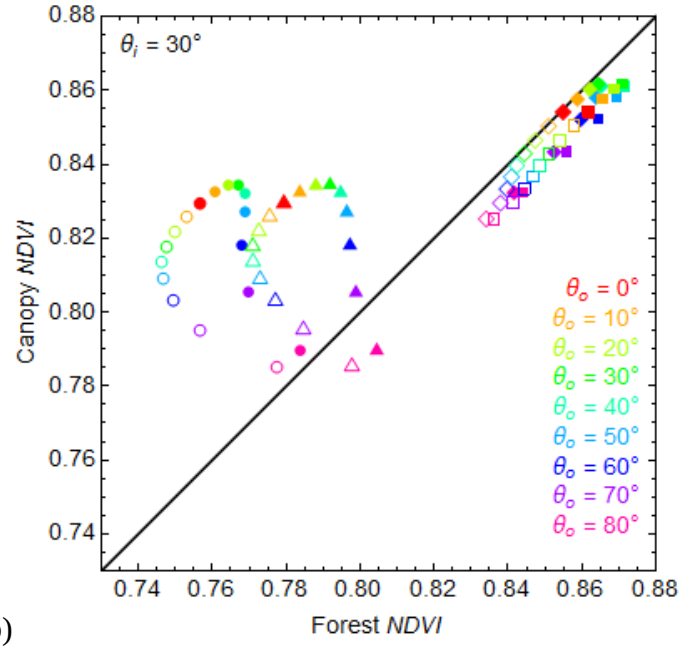

b)

Figure 9. The *NDVI* value of the canopy as a function of the forest *NDVI* value for various values of view zenith angle and the sun zenith angle values 60º (a) and 30º (b). The solid symbols indicate the forward scattering direction and the open symbols the backscattering direction. The markers denote: circles: (LAI = 1, LAI_g =1), triangles: (LAI = 1, LAI_g = 4), diamonds: (LAI = 4, LAI_g = 1), and squares: (LAI = 4, LAI_g = 4).

4. Discussion

The *BRF* model presented here shows that for sparse coniferous forests (Table 1), the contribution of the forest floor to the total *BRF* of the forest can be larger than that of the canopy. But even for denser coniferous forests, the contribution of the forest floor to BRF_f can exceed 5 % and 15% in the red wavelength range and 10 % and 15% in the NIR wavelength range for the sun zenith angle values 60° and 30°, respectively. The effect is larger with smaller view zenith angle values, which is understandable because the forest floor is more visible when viewed from close to nadir. The relative angular variation of BRF_f is rather insensitive to the forest floor in the red wavelength range and at large sun zenith angle values, so that fitting the normalized *BRF* to satellite reflectance values seems a preferable alternative to fitting directly the *BRF* values, when the forest floor properties are not known and the goal is to estimate the canopy *LAI*. In addition, the *BRF* dependence on the azimuth angle difference of the incoming radiation and the viewing direction is in the red wavelength range about the same for the canopy and the forest for sun and view zenith angle values of 60°, but differs in the NIR wavelength range. Hence, one might get some information concerning the forest floor by simulating the canopy *BRF* in the NIR wavelength range on the basis of the observed *BRF* in the red wavelength range and comparing it with the observed *BRF* in the NIR wavelength range.

It is well known that for boreal forests the relationship between satellite based *NDVI* and canopy *LAI* gets poorer during the growing season, but is relatively good in spring right after the snow melt [42, 43, 44, 45, 46, 47]. This can be explained by the model results shown here. After the snow melt, the forest floor is covered with withered vegetation of previous year and it is not green. The understory vegetation starts to grow at the onset of the growing season and later in summer the *NDVI* values of the forests may contain a non-negligible component ($\gtrsim$5 %) from the forest floor. As the forest floor *LAI* values (and thus the spectral reflectance values) are not identical for all forests, it is understandable that the varying forest floor contribution to *NDVI* complicates the relationship of *NDVI* with the canopy *LAI*. The same problem occurs when using satellite based *SR* values directly for canopy *LAI* retrieval. Even when *NDVI* or *SR* are not used for estimating the canopy *LAI* one should recognize that the seasonal variation of these indices does not necessarily describe changes in the canopy only. The forest floor effect on *SR* and *NDVI* is larger when the canopy is sparse and the forest floor vegetation is dense, which is typically the case close to the northern boreal forest edge. But one has to notice that even for mature forests (*LAI* = 4) the effect of the forest floor on *SR* and *NDVI* cannot be neglected.

5. Conclusions

A simple analytical *BRF* model including the contribution from the forest floor is presented. It contains only a few parameters needed in addition to the reflectance values and angular information available for satellite data, thus a large satellite image data set is not required for fitting the model in order to estimate *LAI*. The presented model provides a method to take into account the effect of the forest floor on the total forest reflectance. Yet, the current version of the model with its double integrals is rather heavy to use for inversion of satellite based reflectance values. For operational purposes a LUT based approach would be a practical alternative.

Typical cases of boreal forest were simulated and it was shown that usually the understory vegetation effect on the total forest *BRF* varied within 2 % - 69 % in the red wavelength range

and within 7 % - 54 % in the NIR wavelength range. In addition, it was found that *SR* and *NDVI* values were also sensitive to the forest floor vegetation, especially when the view zenith angle was small. The difference between the forest and canopy values was of the order of 10 % to 30 % for *SR* and of the order of 1 % to 10 % for *NDVI*, depending on the sun and view zenith angles. The relative variations of the canopy and forest *BRFs* with the view angle were mostly alike, only for sparse forest the relationship of the *BRF* with the view angle differed. In addition, the model produced a view angle dependency that has a strong linear relationship with the Ross-thick kernel for dense forests and large sun zenith angle values.

References

1 GCOS (2011), Systematic Observation Requirements for Satellite-Based Products for Climate, 2011 Update, Supplemental Details to the Satellite-Based Component of the Implementation Plan for the Global Observing System for Climate in Support of the UNFCCC (2010 Update), Reference Number GCOS-154, pp. 138, http://www.wmo.int/pages/prog/gcos/Publications/gcos-154.pdf.

2 T.C. Hill, M. Williams, and J.B. Moncrieff, "Modeling feedbacks between a boreal forest and the planetary boundary layer", Journal of Geophysical Research, Vol. 113, D15122, 15 p, 2008.

3 Z.K. Tesemma, Y. Wei, M.C. Peel and A.W. Western, "Including the dynamic relationship between climate variables and leaf area index in a hydrological model to improve streamflow prediction under a changing climate", Hydrol. Earth Syst. Sci, Vol. 19, pp.2821-2836, 2015.

4 A.L. Barbu, Calvet, J.C., Mahfouf, J.F. and Lafont, S, "Integrating ASCAT surface soil moisture and GEOV1 leaf area index into the SURFEX modelling platform: A land data assimilation application over France", Hydrology and Earth System Sciences, Vol. 18, pp. 173-192., 2014.

5 R.A. Betts, , "Offset of the potential carbon sink from boreal forestation by decreases in surface albedo", Nature, Vol. 408, 9 November 2000, pp.187-190, 2000.

6 A. Lindroth, F Lagergren, M. Aurela, B. Bjarnadottir, T. Christensen, E. Dellwik, A. Grelle, A. Ibrom, T. Johansson, H. Lankreijer, S. Launiainen, T. Laurila, M. Mölder, E. Nikinmaa, K. Pilegaard, B.D.. Sigurdsson, and T. Vesala, "Leaf area index is the principal scaling parameter for both gross photosynthesis and ecosystem respiration of Northern deciduous and coniferous forests", Tellus, B60, pp. 129-142, 2008.

7 T. Thum, T. Aalto, T. Laurila, M. Aurela, A. Lindroth, and T. Vesala, "Assessing seasonality of biochemical CO2 exchange model parameters from micrometeorological flux observations at boreal coniferous forest"Biogeosciences, 5, pp. 1625-1639, 2008.

8 C.S. Potter, S. Wang, N.T. Nikolov, A.D. McGuire, J. Liu, A.W. King, J.S. Kimball, R.F. Grant, S.E. Frolking, J.S. Clein, J.M. Chen, J.S. Amthor, "Comparison of boreal ecosystem model sensitivity to variability in climate and forest site parameters", Journal of Geophysical Research, Vol. 106, No. D24, pp. 33671 – 33687, 2001.

9 K.W. and G.B. Bonan, "The Effects of Remotely Sensed Plant Functional Type and Leaf Area Index on Simulations of Boreal Forest Surface Fluxes by the NCAR Land Surface Model", Journal of Hydrometeorology, Vol. 1, pp. 431 – 446, 2000.

10 A. Verger, F. Baret, M. Weiss, I. Filella, and J. Peñuelas, "GEOCLIM: A global climatology of LAI, FAPAR, and FCOVER from VEGETATION observations for 1999-2010", Remote Sensing of Environment, Vol.166, pp. 126-137, 2015.

11 S. Boussetta, G. Balsamo, A. Beljaars, T. Kral, .and L. Jarlan, Impact of a satellite derived leaf area index monthly climatology in a global numerical weather prediction model. International Journal of Remote Sensing, 34, pp. 3520–3542, 2013.
12 H. Fang, C. Jiang, W. Li, S. Wei, F. Baret, J.M. Chen, J. Garcia-Haro, S. Liang, R. Liu, R.B. Myneni, B Pinty, Z. Xiao and Z. Zhu, "Characterization and intercomparison of global moderate resolution leaf area index (LAI) products: Analysis of climatologies and theoretical uncertainties", Journal of Geophysical Research, Vol. 188, pp. 1-20, 2013.
13 J. Knyazikhin, J.V. Martonchik, R.B. Myneni, D.J. Diner and S.W. Running, S.W., "Synergistic algorithm for estimating vegetation canopy leaf area index and fraction of absorbed photosynthetically active radiation from MODIS and MISR data", Journal of Geophysical Research – Vol. 103, No. D24, pp. 32,257-32,275, 1998.
14 R. B. Myneni, S. Hoffman, Y. Knyazikhin, J. L. Privette, J. Glassy, Y. Tian, Y. Wang, X. Song, Y. Zhang, G. R. Smith, A. Lotsch, M. Friedl, J. T. Morisette, P. Votava, R. R. Nemani, and S. W. Running, "Global products of vegetation leaf area and fraction absorbed PAR from year one of MODIS data", Remote Sens. Environ., Vol. 83, No.1–2, pp. 214–231, 2002.
15 D. Huang, Y. Knyazikhin, W. Wang, D. W. Deering, P. Stenberg, N. Shabanov, B. Tan, and R. B. Myneni, , "Stochastic transport theory for investigating the three-dimensional canopy structure from space measurements", Remote Sens. Environ., Vol. 112, No.1, pp- 35–50, 2008.
16 F. Deng, J. M. Chen, S. Plummer, M. Chen, and J. Pisek, "Algorithm for global leaf area index retrieval using satellite imagery", IEEE Trans. Geosci. Remote Sens., Vol. 44, No. 8, pp. 2219–2229, 2006.
17 S. Plummer, O. Arino, M. Simon, and W. Steffen, "Establishing a Earth observation product service for the terrestrial carbon community: The globcarbon initiative", Mitig. Adapt. Strat. Glob. Chang., Vol. 11, No. 1, pp. 97–111, , 2006.
18 F. Baret, O. Hagolle, B. Geiger, P. Bicheron, B. Miras, M. Huc, B. Berthelot, F. Nino, M. Weiss, O. Samain, J.-L. Roujean, M. Leroy, LAI, fPAR, and fCover CYCLOPES global products derived from VEGETATION Part 1: Principles of the algorithm, Remote Sens. Environ., Vol. 110, No.3, pp. 275–286, 2007.
19 J.K. Ross, The radiation Regime and Architecture of Plant Stands, 392 pp., Dr. W. Junk Publishers, The Hague, 1981.
20 J.L. Roujean, M. Leroy and P.Y. Deschamps, "A bidirectional reflectance model of the Earth's surface for the correction of remote sensing data", J. Geophys.Res., Vol. 97, pp.20455-20468, 1992.
21 W. Wanner and A. H., Strahler, "On the derivation of kernels for kernel-driven models of bidirectional reflectance", Journal of Geophysical Research, Vol. 100, No. D10, pp.21077-21089, 1995.
22 X. Li and A. H. Strahler, "Geometric-optical bidirectional reflectance modeling of a conifer forest canopy", IEEE Trans. Geosci. Remote Sens., Vol. 24, pp. 906-919, 1986.
23 X. Li and A. H. Strahler, "Geometric-optical bidirectional reflectance modeling of the discrete crown vegetation canopy: effect of crown shape and mutual shadowing", IEEE Trans. Geosci. Remote Sens., Vol. 30, pp. 276-292, 1992.
24 W. Lucht, C.B. Schaafand A.H. Strahler,"An Algorithm for the retrieval of albedo from space using semiempirical BRDF models", IEEE Trans. Geosci., Remote Sens., Vol.38, pp., 977–998, 2000.
25 C. B. Schaaf,, F. Gao, A. H. Strahler, W. Lucht, X. Li, T. Tsang, N. C. Strugnell, X. Zhang, Y. Jin, J.-P. Muller, P. Lewis, M. Barnsley, P. Hobson, M. Disney, G. Roberts,

M. Dunderdale, C. Doll, R. P. d'Entremont, B. Hu, S. Liang, J. L. Privette, D. Roy, "First operational BRDF, albedo nadir reflectance products from MODIS", Remote Sensing of Environment, Vol. 83, pp. 135–148, 2002.
26 A.K. Cajander, "The theory of forest types", Acta For. Fenn., Vol. 29, pp. 1-108, 1926.
27 W.B. Rossow, and R.A. Schiffer,, "Advances in Understanding Clouds from ISCCP", Bull. Amer. Meteor. Soc., Vol. 80, pp. 2261-2288, 1999.
28 Y. Knyazikhin, M.A. Schull, X. Liang, R.B. Myneni, and A. Samanta, , "Canopy spectral invariants. Part 1: A new concept in remote sensing", Journal of Quantitative Spectroscopy & Radiative Transfer, Vol. 112, pp. 727-735, 2011.
29 S. Smolander and P. Stenberg, "A method to account for shoot scale clumping in coniferous canopy reflectance models", Remote Sensing of Environment, Vol. 88, pp. 363-373, 2003.
30 M. Rautiainen and Stenberg, P., "Application of photon recollision probability in coniferous canopy reflectance simulations", Remote Sensing of Environment, Vol. 96, No. 1, pp. 98–107, 2005.
31 P. Stenberg and T. Manninen, "The effect of clumping on canopy scattering and its directional properties: a model simulation using spectral invariants", International Journal of Remote Sensing, Vol. 36, No. 19-20, pp. 5178-5191, 2015.
32 T. Manninen and Stenberg, P., "Simulation of the effect of snow covered forest floor on the total forest albedo", Agricultural and Forest Meteorology, Vol. 149, pp. 303-319, 2009.
33 M. Rautiainen and Stenberg, P., "On the angular dependency of canopy gap fractions in pine, spruce and birch stands ", Agricultural and Forest Meteorology, Vol. 206, No. 15, pp. 1–3, 2015.
34 P. Stenberg, "Correcting LAI-2000 estimates for the clumping of needles in shoots of conifers", Agricultural and Forest Meteorology, Vol. 79, pp. 1-8, 1996.
35 E.J. Hyer and S.J. Goetz, "Comparison and sensitivity analysis of instruments and radiometric methods for LAI estimation: assessments from a boreal forest site", Agricultural and Forest Meteorology, Vol. 122, pp. 157–174, 2004.
36 P. Stenberg,, "Simple analytical formula for calculating average photon recollision probability in vegetation canopies", Remote Sensing of Environment, Vol. 109, No. 2, pp. 221–224, 2007.
37 G. Schaepman-Strub, M.E. Schaepman, T.H. Painter, S. Dangel and J.V. Martonchik, "Reflectance quantities in optical remote sensing — definitions and case studies", Remote Sensing of Environment Vol. 103, pp. 27 – 42, 2006.
38 J.M. Chen and S.G. Leblanc,"A four-scale bidirectional reflectance model based on canopy architecture", IEEE Transactions on Geoscience and Remote Sensing, Vol. 35, No. 5, pp.1316-1337, 1997.
39 J. M. Chen and J. Cihlar, "A hotspot function in a simple bidirectional reflectance model for satellite applications", Journal of Geophysical Research, Vol. 102, No. D22, pp.25907-25913, 1997.
40 P. Stenberg, M. Rautiainen, T. Manninen, P. Voipio and M. Möttus, "Boreal forest leaf area index from optical satellite images: model simulations and empirical analyses using data from central Finland", Boreal Environment Research Vol. 13, pp. 433-443, 2008.
41 M. Rautiainen, J. Suomalainen, M. Mõttus, P. Stenberg, P. Voipio, J. Peltoniemi, T. Manninen, "Coupling forest canopy and understory reflectance in the Arctic latitudes of Finland", Remote Sensing of Environment, Vol. 110, No. 3, pp. 332-343, 2007.
42 J.M. Chen and J. Cihlar, "Retrieving leaf area index of boreal conifer forests using Landsat TM images", Remote Sensing of Environment Vol. 55, pp. 153–162, 1996.

43 T. Häme, A. Salli, K. Andersson, and A. Lohi, "A new methodology for the estimation of biomass of conifer-dominated boreal forest using NOAA AVHRR data", International Journal of Remote Sensing Vol. 18, No. 15, pp. 3211–3243, 1997.
44 T. Nilson, J. Anniste, M. Lang, and J. Praks, "Determination of needle area indices of forest canopies in the NOPEX region by ground-based optical measurements and satellite images", Agricultural and Forest Meteorology, Vol. 98–99, pp. 449–462, 1999.
45 L. Eklundh, L. Harrieand A. Kuusk, "Investigating relationships between Landsat ETM+ sensor data and leaf area index in boreal conifer forest", Remote Sensing of Environment Vol. 78, pp. 239–251, 2001.
46 M. Rautiainen, P. Stenberg, T. Nilson, A. Kuuskand H. Smolander, "Application of a forest reflectance model in estimating leaf area index of Scots pine stands using Landsat 7 ETM reflectance data",Canadian Journal of Remote Sensing Vol. 29, No. 3, pp. 314–323, 2003.
47 P. Stenberg, M. Rautiainen, T. Manninen, P. Voipio and H. Smolander, "Reduced simple ratio better than NDVI for estimating LAI in Finnish pine and spruce stands", Silva Fennica Vol. 38, No. 1, pp. 3-14, 2004.
48 P. Lukeš, P. Stenberg, M. Rautiainen, M. Mõttus and K.M. Vanhatalo, ”Optical properties of leaves and needles for boreal tree species in Europe”, Remote Sensing Letters, Vol. 4, No. 7, pp.667-676, 2013.
49 P. Lukeš, P. Stenberg, M. Rautiainen, ”Relationship between forest density and albedo in the boreal zone”, Ecological Modelling, Vol. 261-262, pp. 74-79, 2013.
50 J.I. Peltoniemi, S. Kaasalainen, J. Näränen, M. Rautiainen, P. Stenberg, H, Smolander, S. Smolander and P. Voipio, ”BRDF measurement of understorey vegetation in pine forests: dwarf shrubs, lichen, and moss”, Remote Sensing of Environment, Vol. 94, pp. 343-354, 2005.
51 M., Rautiainen and P. Stenberg, “Simplified tree crown model using standard forest mensuration data for Scots pine”, Agricultural and Forest Meteorology Vol. 128, pp. 123-129, 2005.

Appendix A: Nomenclature

b	Vertical semi-axis of the crown ellipsoid
BHR_f	Bi-hemispherical reflectance of the forest, i.e. white-sky albedo
$BHDRF_f(\theta_o, \varphi_o)$	Fraction of the incoming radiation per unit area scattered in direction (θ_o, φ_o)
BRF	Bidirectional reflection factor
BTF	Bidirectional transmittance factor
BRF_c	Bidirectional reflection factor of canopy only
BRF_f	Total bidirectional reflection factor of forest
BRF_g	Bidirectional reflection factor of forest floor vegetation
BRF_{cc}	Bidirectional reflection factor containing contribution only from canopy ($=BRF_c$)
BRF_{cg}	Bidirectional reflection factor containing contributions from canopy and forest floor scattering with last scattering from the floor,
BRF_{gc}	Bidirectional reflection factor containing contributions from canopy and forest floor scattering with last scattering from the canopy
BRF_{gg}	Bidirectional reflection factor containing contribution only forest floor
BRF_1	Bidirectional reflection factor of the first scattering
BRF'_1	Bidirectional reflection factor of the first scattering including the hotspot effect
BTF_1	Bidirectional transmittance factor of the first scattering
c_1 and c_2	Hotspot coefficients
D	Fraction of diffuse irradiance
DHR_1	First order directional hemispherical reflectance
DHR_f	Directional hemispherical reflectance of the forest, i.e. black-sky albedo
$DBHR_f$	Blue-sky albedo of forest
DHT_1	First order directional hemispherical transmittance
Ei	Exponential integral function
f_{iso},	Coefficient of isotropic kernel
f_{geo}	Coefficient of geometric kernel
f_{vol}	Coefficient of volumetric kernel
G	Mean projection of unit leaf (needle) area
h	Distance to the centre of the crown above the ground
$HDRF_f$,	Bi-hemispherical reflectance of forest

$HDRF_{cc}$	Bi-hemispherical reflectance of forest canopy only
$HDRF_{gg}$	Bi-hemispherical reflectance of forest floor only
$HDRF_{gc}$	Bi-hemispherical reflectance of forest containing contributions from canopy and forest floor scattering with last scattering from the canopy
$HDRF_{cg}$	Bi-hemispherical reflectance of forest containing contributions from canopy and forest floor scattering with last scattering from the floor
i_D	Canopy diffuse interceptance
i_0	Canopy interceptance
k	Hotspot effect coefficient
k_{geo}	Geometric kernel
k_{vol}	Volumetric kernel
LAI	Leaf area index
$NDVI$	Normalized difference vegetation index
p	Photon recollision probability
p_1	Photon recollision probability after the first scattering event
p_d	Photon recollision probability of multiple order
r	Horizontal semi-axis of the crown ellipsoid
R^2	Coefficient of determination
$s_d(\theta_i, \theta_1, \varphi_1)$	Directional distribution of radiation incident from zenith angle θ_i scattered from the canopy to the forest floor in the direction (θ_1, φ_1)
$s_g(\theta_i, \theta_1, \varphi_1)$	Directional distribution of the radiation incident from zenith angle θ_i scattered from the forest floor to the canopy in the direction (θ_1, φ_1)
SR	Simple ratio vegetation index
t_0	Uncollided canopy transmittance
β	Canopy clumping index
γ	Phase angle
φ	Azimuth angle of scattered radiation
φ_o	Azimuth angle of the outgoing radiation
θ	Zenith angle of scattered radiation
θ_i	Zenith angle of the incoming radiation
θ_o	Zenith angle of the outgoing radiation
ρ	Reflectance of a leaf
ρ_g	Forest floor reflectance in Ross-thick kernel

ρ_1	Directional escape probability of the first order scattering
ρ_d	Directional escape probability of the diffuse scattering
τ	Transmittance of a leaf
ω_C	Canopy scattering coefficient
ω_L	Leaf single scattering albedo
Ω	Space angle

Appendix B: Approximations of canopy BRF and BTF

Simple analytical approximative functions were derived for the canopy BRF_c and BTF_c (denoted here simply *BRF* and *BTF*) approximating the scattering phase related term $(\cos\gamma\,(-2\gamma\,+\pi)+2\sin\gamma)$ with a polynome of second order in $\cos^2\gamma$, namely: $2+f_1\cos^2\gamma+f_2\,\cos^4\gamma$, where $\cos(\gamma)=u_iu+\sqrt{1-u_i{}^2}\sqrt{1-u^2}\cos\varphi$, u = $\cos\theta$ and u_i = $\cos\theta_i$, θ being the zenith angle of the scattered ray and θ_i the zenith angle of the incoming ray and φ difference of their azimuth angles. The coefficients have the values f_1 = 0.9630536970903564 and f_2 = 0.17163057942426657. The agreement of the approximation is very good (Figure B1).

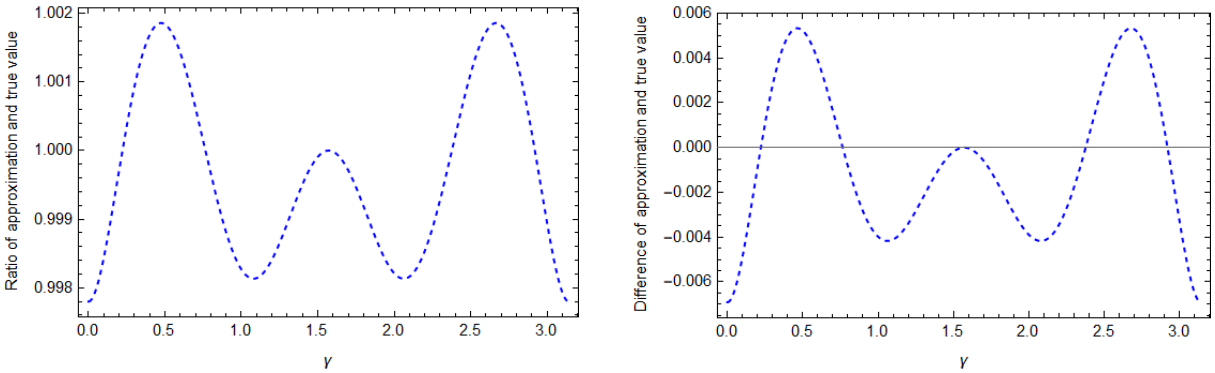

Figure B1. The ratio (left) and difference (right) of the approximative $2+f_1\cos^2\gamma+f_2\,\cos^4\gamma$ and original scattering phase related function $(\cos\gamma\,(-2\gamma\,+\pi)+2\sin\gamma)$.

Applying the above approximation to the phase related term, it is possible to analytically integrate the bidirectional reflectance and transmittance factors of the canopy from first scattering, BRF_1 (Eq. 6) and BTF_1 (Eq. 7) respectively, to derive DHR_1 (Eq. 9) and DHT_1 (Eq. 10). Consequently, the diffuse reflectance BRF_d can also be derived in analytic form (Stenberg and Manninen, 2015) and hence both the total bidirectional reflectance and transmittance (*BRF* and *BTF*) are also derived in analytic form. The approximations of DHR_1 and DHT_1 differed from the numerically integrated values of Eqs. 9 and 10 less than 10^{-8} in the range 0.1…1 of u and u_i.

The explicit formulas are:

$$DHR_1(u_i)=\frac{1}{\pi}\int_0^{2\pi}\int_0^{\frac{\pi}{2}}\frac{\left(1-e^{-\frac{a(u+u_i)}{uu_i}}\right)\omega\beta\left(2+f_1\left(uu_i+\sqrt{1-u^2}\sqrt{1-u_i{}^2}\cos\varphi\right)^2+f_2\left(uu_i+\sqrt{1-u^2}\sqrt{1-u_i{}^2}\cos\varphi\right)^4\right)}{6G\pi(u+u_i)}udud\varphi$$

$$=\frac{\omega\beta}{6G\pi}(R_1+R_2+R_3+R_4+R_5) \qquad \text{(B1)}$$

$$R_1=(r_{10}+r_{11}u_i+r_{12}u_i{}^2+r_{13}u_i{}^3+r_{14}u_i{}^4+r_{15}u_i{}^5+r_{16}u_i{}^6+r_{17}u_i{}^7+r_{18}u_i{}^8)$$

$$r_{10}=4+\frac{2f_1}{3}+\frac{2f_2}{5}$$

$$r_{11} = \frac{f_1}{2} + \frac{9f_2}{16}$$

$$r_{12} = -f_1 - \frac{5f_2}{4}$$

$$r_{13} = -\frac{3f_1}{2} - 3f_2$$

$$r_{14} = 3f_1 + \frac{29f_2}{4}$$

$$r_{15} = \frac{85}{16}f_2$$

$$r_{16} = -\frac{145}{12}f_2$$

$$r_{17} = -\frac{35}{8}f_2$$

$$r_{18} = \frac{35}{4}f_2$$

$$R_2 = e^{-\frac{a(1+u_i)}{u_i}}(r_{20} + r_{21}u_i + r_{22}{u_i}^2 + r_{23}{u_i}^3 + r_{24}{u_i}^4 + r_{25}{u_i}^5 + r_{26}{u_i}^6 + r_{27}{u_i}^7 + r_{28}{u_i}^8)$$

$$r_{20} = -4 - \frac{2f_1}{3} - \frac{af_1}{6} + \frac{1}{6}a^2f_1 - \frac{2f_2}{5} - \frac{17af_2}{80} + \frac{19}{80}a^2f_2 + \frac{1}{160}a^3f_2 - \frac{1}{160}a^4f_2$$

$$r_{21} = -\frac{f_1}{2} + \frac{af_1}{2} - \frac{9f_2}{16} + \frac{11af_2}{16} + \frac{1}{32}a^2f_2 - \frac{1}{32}a^3f_2$$

$$r_{22} = f_1 + \frac{af_1}{2} - \frac{1}{2}a^2f_1 + \frac{5f_2}{4} + \frac{5af_2}{4} - \frac{3}{2}a^2f_2 - \frac{1}{16}a^3f_2 + \frac{1}{16}a^4f_2$$

$$r_{23} = \frac{3f_1}{2} - \frac{3af_1}{2} + 3f_2 - \frac{17af_2}{4} - \frac{5}{16}a^2f_2 + \frac{5}{16}a^3f_2$$

$$r_{24} = -3f_1 - \frac{29f_2}{4} - \frac{33af_2}{16} + \frac{113}{48}a^2f_2 + \frac{7}{96}a^3f_2 - \frac{7}{96}a^4f_2$$

$$r_{25} = -\frac{85f_2}{16} + \frac{325af_2}{48} + \frac{35}{96}a^2f_2 - \frac{35}{96}a^3f_2$$

$$r_{26} = \frac{145f_2}{12} + \frac{35af_2}{24} - \frac{35}{24}a^2f_2$$

$$r_{27} = \frac{35f_2}{8} - \frac{35af_2}{8}$$

$$r_{28} = -\frac{35}{4}f_2$$

$$R_3 = e^{-\frac{a(1+u_i)}{u_i}}\mathrm{Ei}(-a)(r_{30} + r_{31}u_i + r_{32}{u_i}^2 + r_{33}{u_i}^3 + r_{34}{u_i}^4 + r_{35}{u_i}^5 + r_{36}{u_i}^6 + r_{37}{u_i}^7 + r_{38}{u_i}^8 + r_{39}{u_i}^9)$$

$$r_{30} = -4ae^a - ae^af_1 + \frac{1}{6}a^3e^af_1 - \frac{3}{4}ae^af_2 + \frac{1}{4}a^3e^af_2 - \frac{1}{160}a^5e^af_2$$

$$r_{31} = -4e^a - e^af_1 + \frac{1}{2}a^2e^af_1 - \frac{3}{4}e^af_2 + \frac{3}{4}a^2e^af_2 - \frac{1}{32}a^4e^af_2$$

$$r_{32} = 2ae^af_1 - \frac{1}{2}a^3e^af_1 + 3ae^af_2 - \frac{13}{8}a^3e^af_2 + \frac{1}{16}a^5e^af_2$$

$$r_{33} = 2e^a f_1 - \frac{3}{2}a^2 e^a f_1 + 3e^a f_2 - \frac{39}{8}a^2 e^a f_2 + \frac{5}{16}a^4 e^a f_2$$

$$r_{34} = -3ae^a f_1 - \frac{21}{2}ae^a f_2 + \frac{5}{2}a^3 e^a f_2 - \frac{7}{96}a^5 e^a f_2$$

$$r_{35} = -3e^a f_1 - \frac{21}{2}e^a f_2 + \frac{15}{2}a^2 e^a f_2 - \frac{35}{96}a^4 e^a f_2$$

$$r_{36} = 15ae^a f_2 - \frac{35}{24}a^3 e^a f_2$$

$$r_{37} = 15e^a f_2 - \frac{35}{8}a^2 e^a f_2$$

$$r_{38} = -\frac{35}{4}ae^a f_2$$

$$r_{39} = -\frac{35}{4}e^a f_2$$

$$R_4 = \mathrm{Ei}\left(-\frac{a(1+u_i)}{u_i}\right)(r_{41}u_i + r_{43}{u_i}^3 + r_{45}{u_i}^5 + r_{47}{u_i}^7 + r_{49}{u_i}^9)$$

$$r_{41} = 4 + f_1 + \frac{3}{4}f_2$$

$$r_{43} = -2f_1 - 3f_2$$

$$r_{45} = 3f_1 + \frac{21}{2}f_2$$

$$r_{47} = -15f_2$$

$$r_{49} = \frac{35}{4}f_2$$

$$R_5 = \mathrm{Log}\left(\frac{u_i}{1+u_i}\right)(r_{51}u_i + r_{53}{u_i}^3 + r_{55}{u_i}^5 + r_{57}{u_i}^7 + r_{59}{u_i}^9)$$

$$r_{51} = 4 + f_1 + \frac{3f_2}{4}$$

$$r_{53} = -2f_1 - 3f_2$$

$$r_{55} = 3f_1 + \frac{21f_2}{2}$$

$$r_{57} = -15f_2$$

$$r_{59} = \frac{35}{4}f_2$$

$$DHT_1(u_i) =$$

$$\frac{1}{\pi}\int_0^{2\pi}\int_0^{\frac{\pi}{2}} \frac{(e^{-\frac{a}{u}} - e^{-\frac{a}{u_i}})\omega\beta\left(2 + f_1\left(uu_i + \sqrt{1-u^2}\sqrt{1-{u_i}^2}\cos\varphi\right)^2 + f_2\left(uu_i + \sqrt{1-u^2}\sqrt{1-{u_i}^2}\cos\varphi\right)^4\right)}{6G\pi(u-u_i)} u\,du\,d\varphi$$

$$= \frac{e^{-\frac{a(1+u_i)}{u_i}}\omega\beta}{2880G\pi}(T_1 + T_2 + T_3 + T_4) \qquad \text{(B2)}$$

$$T_1 = (t_{10} + t_{11}u_i + t_{12}{u_i}^2 + t_{13}{u_i}^3 + t_{14}{u_i}^4 + t_{15}{u_i}^5 + t_{16}{u_i}^6 + t_{17}{u_i}^7 + t_{18}{u_i}^8)$$

$$t_{10} = -1920e^a - 320e^a f_1 - 192e^a f_2$$

$$t_{11} = 240e^a f_1 + 270e^a f_2$$

$$t_{12} = 480e^a f_1 + 600e^a f_2$$

$$t_{13} = -720e^a f_1 - 1440e^a f_2$$

$$t_{14} = -1440e^a f_1 - 3480e^a f_2$$

$$t_{15} = 2550e^a f_2$$

$$t_{16} = 5800e^a f_2$$

$$t_{17} = -2100e^a f_2$$

$$t_{18} = -4200e^a f_2$$

$$T_2 = e^{a/u_i}(t_{20} + t_{21}u_i + t_{22}{u_i}^2 + t_{23}{u_i}^3 + t_{24}{u_i}^4 + t_{25}{u_i}^5 + t_{26}{u_i}^6 + t_{27}{u_i}^7 + t_{28}{u_i}^8)$$

$$t_{20} = 1920 + 320f_1 + 80af_1 - 80a^2 f_1 + 192f_2 + 102af_2 - 114a^2 f_2 - 3a^3 f_2 + 3a^4 f_2$$

$$t_{21} = -240f_1 + 240af_1 - 270f_2 + 330af_2 + 15a^2 f_2 - 15a^3 f_2$$

$$t_{22} = -480f_1 - 240af_1 + 240a^2 f_1 - 600f_2 - 600af_2 + 720a^2 f_2 + 30a^3 f_2 - 30a^4 f_2$$

$$t_{23} = 720f_1 - 720af_1 + 1440f_2 - 2040af_2 - 150a^2 f_2 + 150a^3 f_2$$

$$t_{24} = 1440f_1 + 3480f_2 + 990af_2 - 1130a^2 f_2 - 35a^3 f_2 + 35a^4 f_2$$

$$t_{25} = -2550f_1 + 3250af_2 + 175a^2 f_2 - 175a^3 f_2$$

$$t_{26} = -5800f_2 - 700af_2 + 700a^2 f_2$$

$$t_{27} = 2100f_2 - 2100af_2$$

$$t_{28} = 4200f_2$$

$$T_3 = e^{\frac{a(1+u_i)}{u_i}}\,\mathrm{Ei}(-a)(t_{30} + t_{31}u_i + t_{32}{u_i}^2 + t_{33}{u_i}^3 + t_{34}{u_i}^4 + t_{35}{u_i}^5 + t_{36}{u_i}^6 + t_{37}{u_i}^7 + t_{38}{u_i}^8 + t_{39}{u_i}^9)$$

$$t_{30} = 1920a + 480af_1 - 80a^3 f_1 + 360af_2 - 120a^3 f_2 + 3a^5 f_2$$

$$t_{31} = -1920 - 480f_1 + 240a^2 f_1 - 360f_2 + 360a^2 f_2 - 15a^4 f_2$$

$$t_{32} = -960af_1 + 240a^3 f_1 - 1440af_2 + 780a^3 f_2 - 30a^5 f_2$$

$$t_{33} = 960f_1 - 720a^2 f_1 + 1440f_2 - 2340a^2 f_2 + 150a^4 f_2$$

$$t_{34} = 1440af_1 + 5040af_2 - 1200a^3 f_2 + 35a^5 f_2$$

$$t_{35} = -1440f_1 - 5040f_2 + 3600a^2 f_2 - 175a^4 f_2$$

$$t_{36} = -7200af_2 + 700a^3f_2$$

$$t_{37} = 7200f_2 - 2100a^2f_2$$

$$t_{38} = 4200af_2$$

$$t_{39} = -4200f_2$$

$$T_4 = \mathrm{Ei}\left(a(-1+\frac{1}{u_i})\right)(t_{41}u_i + t_{43}{u_i}^3 + t_{45}{u_i}^5 + t_{47}{u_i}^7 + t_{49}{u_i}^9)$$

$$t_{41} = 1920e^a + 480e^af_1 + 360e^af_2$$

$$t_{43} = -960e^af_1 - 1440e^af_2$$

$$t_{45} = 1440e^af_1 + 5040e^af_2$$

$$t_{47} = -7200e^af_2$$

$$t_{49} = 4200e^af_2$$

$$T_5 = \mathrm{Log}\left(\frac{u_i}{1-u_i}\right)(t_{51}u_i + t_{53}{u_i}^3 + t_{55}{u_i}^5 + t_{57}{u_i}^7 + t_{59}{u_i}^9)$$

$$t_{51} = 1920e^a + 480e^af_1 + 360e^af_2$$

$$t_{53} = -960e^af_1 - 1440e^af_2$$

$$t_{55} = 1440e^af_1 + 5040e^af_2$$

$$t_{57} = -7200e^af_2$$

$$t_{59} = 4200e^af_2$$

The analytic integrals of DHR_1 and DHT_1 match the corresponding numerical integrals of Eqs. 6 and 7in the range $u_i = 0.1 \ldots 1$ with an accuracy better than 10^{-8}.

$$BRF_d(\Omega) = \frac{(1-e^{-\mathrm{a}/u})(1-e^{-\mathrm{a}/u_i})G\boldsymbol{\beta}\omega^2\left(1-\frac{\beta}{2880(1-e^{-\mathrm{a}/u_i})G\pi}(D_1+D_2+D_3+D_4+D_5+D_6+D_7+D_8+D_9)\right)}{2\pi(a-a\omega+G\beta\omega e^{-a}(-1+a+e^a+a^2e^a\mathrm{Ei}(-a)))}$$

$$D_1 = d_{10} + d_{11}u_i + d_{12}{u_i}^2 + d_{13}{u_i}^3 + d_{14}{u_i}^4 + d_{15}{u_i}^5 + d_{16}{u_i}^6 + d_{17}{u_i}^7 + d_{18}{u_i}^8$$

$$d_{10} = 1920 + 320f_1 + 192f_2$$

$$d_{11} = 240f_1 + 270f_2$$

$$d_{12} = -480f_1 - 600f_2$$

$$d_{13} = -720f_1 - 1440f_2$$

$$d_{14} = 1440f_1 + 3480f_2$$

$$d_{15} = 2550f_2$$

$$d_{16} = -5800f_2$$

$$d_{17} = -2100f_2$$

$$d_{18} = 4200f_2$$

$$D_2 = e^{-a}(d_{20} + d_{21}u_i + d_{22}{u_i}^2 + d_{23}{u_i}^3 + d_{24}{u_i}^4 + d_{25}{u_i}^5 + d_{26}{u_i}^6 + d_{27}{u_i}^7 + d_{28}{u_i}^8)$$

$$d_{20} = 1920 + 320f_1 + 80af_1 - 80a^2f_1 + 192f_2 + 102af_2 - 114a^2f_2 - 3a^3f_2 + 3a^4f_2$$

$$d_{21} = -240f_1 + 240af_1 - 270f_2 + 330af_2 + 15a^2f_2 - 15a^3f_2$$

$$d_{22} = -480f_1 - 240af_1 + 240a^2f_1 - 600f_2 - 600af_2 + 720a^2f_2 + 30a^3f_2 - 30a^4f_2$$

$$d_{23} = 720f_1 - 720af_1 + 1440f_2 - 2040af_2 - 150a^2f_2 + 150a^3f_2$$

$$d_{24} = 1440f_1 + 3480f_2 + 990af_2 - 1130a^2f_2 - 35a^3f_2 + 35a^4f_2$$

$$d_{25} = -2550f_2 + 3250af_2 + 175a^2f_2 - 175a^3f_2$$

$$d_{26} = -5800f_2 - 700af_2 + 700a^2f_2$$

$$d_{27} = 2100f_2 - 2100af_2$$

$$d_{28} = 4200f_2$$

$$D_3 = e^{-\frac{a(1+u_i)}{u_i}}(d_{30} + d_{31}u_i + d_{32}{u_i}^2 + d_{33}{u_i}^3 + d_{34}{u_i}^4 + d_{35}{u_i}^5 + d_{36}{u_i}^6 + d_{37}{u_i}^7 + d_{38}{u_i}^8)$$

$$d_{30} = -1920 - 1920e^a - 320f_1 - 80af_1 + 80a^2f_1 - 320e^af_1 - 192f_2 - 102af_2 + 114a^2f_2 + 3a^3f_2 - 3a^4f_2 - 192e^af_2$$

$$d_{31} = -240f_1 + 240af_1 + 240e^af_1 - 270f_2 + 330af_2 + 15a^2f_2 - 15a^3f_2 + 270e^af_2$$

$$d_{32} = 480f_1 + 240af_1 - 240a^2f_1 + 480e^af_1 + 600f_2 + 600af_2 - 720a^2f_2 - 30a^3f_2 + 30a^4f_2 + 600e^af_2$$

$$d_{33} = 720f_1 - 720af_1 - 720e^af_1 + 1440f_2 - 2040af_2 - 150a^2f_2 + 150a^3f_2 - 1440e^af_2$$

$$d_{34} = -1440f_1 - 1440e^af_1 - 3480f_2 - 990af_2 + 1130a^2f_2 + 35a^3f_2 - 35a^4f_2 - 3480e^af_2$$

$$d_{35} = -2550f_2 + 3250af_2 + 175a^2f_2 - 175a^3f_2 + 2550e^af_2$$

$$d_{36} = 5800f_2 + 700af_2 - 700a^2f_2 + 5800e^af_2$$

$$d_{37} = 2100f_2 - 2100af_2 - 2100e^af_2$$

$$d_{38} = -4200f_2 - 4200e^af_2$$

$$D_4 = \mathrm{Ei}(-a)e^{-a}(d_{40} + d_{41}u_i + d_{42}{u_i}^2 + d_{43}{u_i}^3 + d_{44}{u_i}^4 + d_{45}{u_i}^5 + d_{46}{u_i}^6 + d_{47}{u_i}^7 + d_{48}{u_i}^8 + d_{49}{u_i}^9)$$

$$d_{40} = 1920ae^a + 480ae^a f_1 - 80a^3e^a f_1 + 360ae^a f_2 - 120a^3e^a f_2 + 3a^5e^a f_2$$

$$d_{41} = -1920e^a - 480e^a f_1 + 240a^2e^a f_1 - 360e^a f_2 + 360a^2e^a f_2 - 15a^4e^a f_2$$

$$d_{42} = -960ae^a f_1 + 240a^3e^a f_1 - 1440ae^a f_2 + 780a^3e^a f_2 - 30a^5e^a f_2$$

$$d_{43} = 960e^a f_1 - 720a^2e^a f_1 + 1440e^a f_2 - 2340a^2e^a f_2 + 150a^4e^a f_2$$

$$d_{44} = 1440ae^a f_1 + 5040ae^a f_2 - 1200a^3e^a f_2 + 35a^5e^a f_2$$

$$d_{45} = -1440e^a f_1 - 5040e^a f_2 + 3600a^2e^a f_2 - 175a^4e^a f_2$$

$$d_{46} = -7200ae^a f_2 + 700a^3e^a f_2$$

$$d_{47} = 7200e^a f_2 - 2100a^2e^a f_2$$

$$d_{48} = 4200ae^a f_2$$

$$d_{49} = -4200e^a f_2$$

$$D_5 = \mathrm{Ei}(-a)e^{-\frac{a(1+u_i)}{u_i}}(d_{50} + d_{51}u_i + d_{52}{u_i}^2 + d_{53}{u_i}^3 + d_{54}{u_i}^4 + d_{55}{u_i}^5 + d_{56}{u_i}^6 + d_{57}{u_i}^7 + d_{58}{u_i}^8 + d_{59}{u_i}^9)$$

$$d_{50} = -1920ae^a - 480ae^a f_1 + 80a^3e^a f_1 - 360ae^a f_2 + 120a^3e^a f_2 - 3a^5e^a f_2$$

$$d_{51} = -1920e^a - 480e^a f_1 + 240a^2e^a f_1 - 360e^a f_2 + 360a^2e^a f_2 - 15a^4e^a f_2$$

$$d_{52} = 960ae^a f_1 - 240a^3e^a f_1 + 1440ae^a f_2 - 780a^3e^a f_2 + 30a^5e^a f_2$$

$$d_{53} = 960e^a f_1 - 720a^2e^a f_1 + 1440e^a f_2 - 2340a^2e^a f_2 + 150a^4e^a f_2$$

$$d_{54} = -1440ae^a f_1 - 5040ae^a f_2 + 1200a^3e^a f_2 - 35a^5e^a f_2$$

$$d_{55} = -1440e^a f_1 - 5040e^a f_2 + 3600a^2e^a f_2 - 175a^4e^a f_2$$

$$d_{56} = 7200ae^a f_2 - 700a^3e^a f_2$$

$$d_{57} = 7200e^a f_2 - 2100a^2e^a f_2$$

$$d_{58} = -4200ae^a f_2$$

$$d_{59} = -4200e^a f_2$$

$$D_6 = \mathrm{Ei}\left(a(-1 + \frac{1}{u_i})\right)e^{-\frac{a(1+u_i)}{u_i}}(d_{61}u_i + d_{63}{u_i}^3 + d_{65}{u_i}^5 + d_{67}{u_i}^7 + d_{69}{u_i}^9)$$

$$d_{61} = 1920e^a + 480e^a f_1 + 360e^a f_2$$

$$d_{63} = -960e^a f_1 - 1440e^a f_2$$

$$d_{65} = 1440e^a f_1 + 5040e^a f_2$$

$$d_{67} = -7200e^a f_2$$

$$d_{69} = 4200e^{a}f_2$$

$$D_7 = \mathrm{Ei}\left(-\frac{a(1+u_i)}{u_i}\right)e^{-a}(d_{71}u_i + d_{73}{u_i}^3 + d_{75}{u_i}^5 + d_{77}{u_i}^7 + d_{79}{u_i}^9)$$

$$d_{71} = 1920e^{a} + 480e^{a}f_1 + 360e^{a}f_2$$

$$d_{73} = -960e^{a}f_1 - 1440e^{a}f_2$$

$$d_{75} = 1440e^{a}f_1 + 5040e^{a}f_2$$

$$d_{77} = -7200e^{a}f_2$$

$$d_{79} = 4200e^{a}f_2$$

$$D_8 = \mathrm{Log}\left(\frac{u_i}{1-u_i}\right)e^{-\frac{a(1+u_i)}{u_i}}(d_{81}u_i + d_{83}{u_i}^3 + d_{85}{u_i}^5 + d_{87}{u_i}^7 + d_{89}{u_i}^9)$$

$$d_{81} = 1920e^{a} + 480e^{a}f_1 + 360e^{a}f_2$$

$$d_{83} = -960e^{a}f_1 - 1440e^{a}f_2$$

$$d_{85} = 1440e^{a}f_1 + 5040e^{a}f_2$$

$$d_{87} = -7200e^{a}f_2$$

$$d_{89} = 4200e^{a}f_2$$

$$D_9 = \mathrm{Log}\left(\frac{u_i}{1+u_i}\right)(d_{91}u_i + d_{93}{u_i}^3 + d_{95}{u_i}^5 + d_{97}{u_i}^7 + d_{99}{u_i}^9)$$

$$d_{91} = 1920 + 480f_1 + 360f_2$$

$$d_{93} = -960f_1 - 1440f_2$$

$$d_{95} = 1440f_1 + 5040f_2$$

$$d_{97} = -7200f_2$$

$$d_{99} = 4200f_2$$

Finally, the total bidirectional reflectance *BRF(Ω)* and transmittance *BTF(Ω)* are

$$BRF(\Omega) = BRF_1(\Omega) + BRF_d(\Omega)$$

$$BTF(\Omega) = BTF_1(\Omega) + BRF_d(\Omega)$$

Appendix C: Solving s_d and s_g

The radiation components scattered from the canopy to the forest floor and the other way round have to be self-consistent, hence we substitute the Eq. 24 to Eq. 23 to obtain

$$s_d(\theta_i,\theta_1,\varphi_1) = BTF_c(\theta_i,\theta_1,\varphi_1) + \int_0^{2\pi}\int_0^{\frac{\pi}{2}} \left(t_0(\theta_i) BRF_g(\theta_i,\theta_2,\varphi_2)\right) BRF_c(\theta_2,\theta_1,\varphi_1-\varphi_2)\cos\theta_2 \sin\theta_2\, d\theta_2 d\varphi_2$$
$$+ \int_0^{2\pi}\int_0^{\frac{\pi}{2}} \left(\int_0^{2\pi}\int_0^{\frac{\pi}{2}} s_d(\theta_i,\theta_3,\varphi_3) BRF_g(\theta_3,\theta_2,\varphi_2-\varphi_3)\cos\theta_3 \sin\theta_3\, d\theta_3 d\varphi_3 \right) BRF_c(\theta_2,\theta_1,\varphi_1-\varphi_2)\cos\theta_2 \sin\theta_2\, d\theta_2 d\varphi_2 \quad \text{(B3)}$$

Now s_d is derived as a function of itself and the self-consistency condition can be applied by multiplying both sides of Eq. B3 by $\cos\theta_1$ and integrating over angles θ_1 and φ_1.

$$\int_0^{2\pi}\int_0^{\pi/2} s_d(\theta_i,\theta_1,\varphi_1)\cos\theta_1\sin\theta_1\,d\theta_1 d\varphi_1$$

$$= \int_0^{2\pi}\int_0^{\pi/2} BTF_c(\theta_i,\theta_1,\varphi_1)\cos\theta_1\sin\theta_1\,d\theta_1 d\varphi_1$$

$$+ \int_0^{2\pi}\int_0^{\pi/2}\left(\int_0^{2\pi}\int_0^{\frac{\pi}{2}}\Big(t_0(\theta_i)BRF_g(\theta_i,\theta_2,\varphi_2)\Big)BRF_c(\theta_2,\theta_1,\varphi_1-\varphi_2)\cos\theta_2\sin\theta_2\,d\theta_2 d\varphi_2\right)\cos\theta_1\sin\theta_1\,d\theta_1 d\varphi_1$$

$$+ \int_0^{2\pi}\int_0^{\pi/2}\left(\int_0^{2\pi}\int_0^{\frac{\pi}{2}}\left(\int_0^{2\pi}\int_0^{\frac{\pi}{2}} s_d(\theta_i,\theta_3,\varphi_3)BRF_g(\theta_3,\theta_2,\varphi_2-\varphi_3)\cos\theta_3\sin\theta_3\,d\theta_3 d\varphi_3\right)BRF_c(\theta_2,\theta_1,\varphi_1 - \varphi_2)\cos\theta_2\sin\theta_2\,d\varphi_2 d\theta_2\right)\cos\theta_1\sin\theta_1\,d\theta_1 d\varphi_1 \quad \text{(B4)}$$

Since all three zenith and azimuth angles are integrated away from the last term of Eq. B4, that term has no angular dependence left and the integration parameters (θ_1, φ_1) and (θ_3, φ_3) of that term can be interchanged. Then we have the following relationship for the integrands on both sides of Eq. B4.

$$s_d(\theta_i,\theta_1,\varphi_1) = BTF_c(\theta_i,\theta_1,\varphi_1) + \int_0^{2\pi}\int_0^{\frac{\pi}{2}}\Big(t_0(\theta_i)BRF_g(\theta_i,\theta_2,\varphi_2)\Big)BRF_c(\theta_2,\theta_1,\varphi_1-\varphi_2)\cos\theta_2\sin\theta_2\,d\theta_2 d\varphi_2$$

$$+ s_d(\theta_i,\theta_1,\varphi_1)\int_0^{2\pi}\int_0^{\frac{\pi}{2}}\int_0^{2\pi}\int_0^{\frac{\pi}{2}} BRF_g(\theta_1,\theta_2,\varphi_2-\varphi_1)\,BRF_c(\theta_2,\theta_3,\varphi_3-\varphi_2)\cos\theta_2\sin\theta_2\cos\theta_3\sin\theta_3\,d\theta_2 d\varphi_2 d\theta_3 d\varphi_3 \quad \text{(B5)}$$

Solving the equation for s_d we get

$$s_d(\theta_i,\theta_1,\varphi_1) = \left(BTF_c(\theta_i,\theta_1,\varphi_1) + t_0(\theta_i)\int_0^{2\pi}\int_0^{\frac{\pi}{2}} BRF_c(\theta_2,\theta_1,\varphi_1-\varphi_2)BRF_g(\theta_i,\theta_2,\varphi_2)\cos\theta_2\sin\theta_2\, d\theta_2 d\varphi_2\right) /$$
$$\left(1 - 1/4\int_0^{2\pi}\int_0^{\frac{\pi}{2}}\int_0^{2\pi}\int_0^{\frac{\pi}{2}} BRF_c(\theta_2,\theta_3,\varphi_3-\varphi_2)BRF_g(\theta_1,\theta_2,\varphi_2-\varphi_1)\cos\theta_2\sin\theta_2\cos\theta_3\sin\theta_3\, d\theta_2 d\varphi_2 d\theta_3 d\varphi_3\right) \quad \text{(B6)}$$

Likewise we substitute Eq. 23 to Eq. 24 in order to get s_g as a function s_g. Applying the self-consistency condition and changing integration parameters as before we get the following equation for the fraction of radiation scattered from the forest floor to the canopy

$$s_g(\theta_i,\theta_1,\varphi_1) = (1-t_0(\theta_1)^2)\left(t_0(\theta_i)BRF_g(\theta_i,\theta_1,\varphi_1) + \int_0^{2\pi}\int_0^{\frac{\pi}{2}} BTF_c(\theta_i,\theta_2,\varphi_2)BRF_g(\theta_2,\theta_1,\varphi_1-\varphi_2)\cos\theta_2\sin\theta_2\, d\theta_2 d\varphi_2\right) /$$
$$\left(\left(1-t_0(\theta_1)\right) - 1/4\int_0^{2\pi}\int_0^{\frac{\pi}{2}}\int_0^{2\pi}\int_0^{\frac{\pi}{2}} BRF_c(\theta_1,\theta_3,\varphi_3-\varphi_1)\, BRF_g(\theta_3,\theta_2,\varphi_2-\varphi_3)\left(1-t_0(\theta_2)\right)\cos\theta_2\sin\theta_2\cos\theta_3\sin\theta_3\, d\theta_2 d\varphi_2 d\theta_3 d\varphi_3\right) \quad \text{(B7)}$$

For convenience we have interchanged the indices 1 and 2 of the angular variables of s_g.

ILMATIETEEN LAITOS
METEOROLOGISKA INSTITUTET
FINNISH METEOROLOGICAL INSTITUTE

FINNISH METEOROLOGICAL INSTITUTE
Erik Palménin aukio 1
P.O. Box 503
FI-00560 HELSINKI
tel. +358 29 539 1000
WWW.FMI.FI

FINNISH METEOROLOGICAL INSTITUTE
REPORTS 2021:5
ISSN 0782-6079
ISBN 978-952-336-137-9 (pdf)
https://doi.org/10.35614/isbn.9789523361379

Helsinki 2021